Calculation of radiation patterns of reflector antennas by high/frequency asymptotic techniques

th e

Calculation of radiation patterns

of reflector antennas

by high-frequency asymptotic techniques

by

M. Safak

Technische Hogeschool Eindhoven
Eindhoven Nederland
Afdeling Elektrotechniek

Eindhoven University of Technology
Eindhoven Netherlands
Department of Electrical Engineering

Calculation of radiation patterns of reflector antennas by high-frequency asymptotic techniques

by

M. Safak

T.H. Report 76-E-62
March 1976

ISBN 90 6144 062 9

Abstract

Radiation pattern of a focus-fed paraboloid is calculated by asymptotic physical optics (APO) and geometrical theory of diffraction (GTD) for dipole and Huygens source feeds. It is shown that the GTD diffraction coefficients are approximations to the PO diffraction coefficients and are valid only in the proximity of the shadow and reflection boundaries. Some errors in the calculation of GTD diffraction coefficients are corrected. Rear radiation is calculated by another asymptotic expansion of the physical optics integral and is compared with the results obtained by other asymptotic techniques. This new expansion is finite in the back direction of the antenna where other methods diverge. Also front to back ratio of a paraboloid, ratio of front radiation to back radiation, is derived by using this new expansion and the results are compared with those predicted by equivalent edge currents method.

TABLE OF CONTENTS PAGE

1. Introduction

Aimer et penser: c'est la veritable
vie des esprits. Voltaire.

The physical optics (PO) approximates the currents on the reflector of a reflector antenna system by the currents calculated from the theory of Geometrical Optics (GO) and uses this current distribution for determining the scattered field. This formulation, involving two dimensional phase integrals with rapidly varying kernels, generally requires lengthy and costly numerical integration. Moreover, it does not satisfy the reciprocity theorem except at a distant axial point in focused condition [1]. In spite of its approximate nature and other shortcomings, PO has been proven very successful in the analysis of reflector antennas.

When the radiating reflector is large compared to wavelength, the scattering process lends itself to a simple geometrical interpretation in terms of reflected and diffracted rays satisfying Keller's extended version of Fermat's principle. This method, initated by Keller ([2], [3]) and known as the Geometrical Theory of Diffraction (GTD), is based on the asymptotic solution of wave equation for a plane wave incident to the edge of a perfectly conducting straight half plane ([4] to [6]). Assuming that, at high frequencies, a curved edge locally behaves like a straight half plane and the incident field is approximately a uniform plane wave, the GTD is systematically applied for finding scattered fields from curved reflectors as well. GTD, in the last decade, has been very popular and is extensively used in the calculation of antenna radiation patterns ([7] to [10]).

Asymptotic nature of GTD also raised the question on the possibilities of applying asymptotic techniques to evaluate the phase integrals widely encountered in the antenna theory. In this context, Rusch evaluated the physical optics integral asymptotically [8]. His solution which is singular at the reflection boundary has been recently improved by Knop [11]. This method of approximating the physical optics integral is known as the asymptotic physical optics (APO). The first order approximation to the PO field is found to come from two stationary points located at the intersection of the Φ-plane containing the observation point and the reflector edge. These two stationary points satisfy Keller's extension of Fermat's principle and consequently coincide with the diffracting edge points determined by the GTD.

The object of this report is to investigate the differences and similarities between the GTD solution, simulating a curved reflector by a straight half plane and assuming an incident plane wave, and the APO solution which approximates the surface current distribution by geometrical optics. Of-course neither of them is exact for calculating the radiation from reflector antennas but they are easy to handle and do not require large computer time as PO does. For this reason, these asymptotic techniques constitute powerful tools in the analysis of large reflector antennas.

In Chapter 2, feed radiation which illuminates the reflector surface and provides direct radiation in the spillover region is studied. Two main feed polarizations considered are those of a Huygens source and of a dipole. Only the $\cos^n\theta$ feed patterns and the one yielding uniform aperture distribution are studied but the analysis can easily be extended to the feeds having different patterns and polarizations.

In the present work, only the paraboloid reflector is considered but the methods employed are applicable to other reflector configurations as well.

In Chapter 3, GTD diffraction coefficients and scattered fields are calculated. It is observed that GTD radiation field is discontinuous at the reflection boundary and yiels erroneous results in the shadow region. Chapter 4 deals with the asymptotic solutions of the physical optics integral and their comparison with the GTD scattered field. It is shown that GTD diffraction coefficients are nothing but the special case of the PO diffraction coefficients and they yield correct results only in the neighborhood of reflection and shadow boundaries. Furthermore, it is confirmed that in the vicinity of the braodside direction, the scalar aperture field method avoids complex phase integration and yields good results. The radiated field in the rear caustic region is found by another asymptotic expansion of the physical optics integral. This formulation is finite at rear caustic unlike the other asymptotic solutions and is conceptually the same as the equivalent edge currents method generally used to calculate the rear radiation ([6] and [12] to [14]). The latter, derived from GTD yielding erroneous results in the shadow region, is not reliable other than being cumbersome. The front/back ratio of a paraboloid (the ratio of front radiation to back radiation), which is important in minimizing the antenna noise and the interference between communication systems, is studied as a function of some antenna parameters. Furthermore, the effect of edge illumination to the antenna gain and to the sidelobe levels is investigated.

2. Feed Radiation

2.1. Incident source field on the paraboloidal surface

Geometry of a front-fed paraboloidal reflector antenna is shown in Fig. 2.1. Let us assume that the incident field on the paraboloidal surface due to a feed located at the focus (F) is given by

$$\bar{E}_f(\rho,\theta,\phi) = A\frac{e^{-jk\rho}}{\rho}\left(\sqrt{G_{f\theta}(\theta,\phi)}\sin\phi\ \hat{\theta} + \sqrt{G_{f\phi}(\theta,\phi)}\ \cos\phi\ \hat{\phi}\right) \tag{2.1}$$

where A is a normalization constant and $G_{f\theta}$ and $G_{f\phi}$ stand for the E-plane and H-plane feed power patterns respectively. On the other hand, from the paraboloid geometry

$$\rho = \frac{2f}{1+\cos\theta} = \rho_0\ \frac{\cos^2\frac{\alpha}{2}}{\cos^2\frac{\theta}{2}} \tag{2.2}$$

Commenly considered feed patterns do not depend upon the variable ϕ; if we take

$$G_{f\theta}(\theta,\phi) = G_{f\phi}(\theta,\phi) = G_f(\theta)$$

Eq. 2.1. can readily be written as

$$\bar{E}_f(\rho,\theta,\phi) = A\frac{e^{-jk\rho}}{\rho}\sqrt{G_f(\theta)}\ \left(\sin\phi\ \hat{\theta} + \cos\phi\ \hat{\phi}\right) \tag{2.3}$$

which represents a feed having Huygens source polarization characteristics with a $\hat{y}$-directed electric field vector.

If E- and H-plane feed patterns satisfy the relation

$$\sqrt{G_{f\theta}(\theta,\phi)} = \sqrt{G_{f\phi}(\theta,\phi)}\ \cos\theta = \sqrt{G_f(\theta)}\ \cos\theta$$

then the electric field vector of the feed may be rewritten as

$$\bar{E}_f(\rho,\theta,\phi) = A\frac{e^{-jk\rho}}{\rho}\sqrt{G_f(\theta)}\ \left(\cos\theta\sin\phi\ \hat{\theta} + \cos\phi\ \hat{\phi}\right) \tag{2.4}$$

which has the polarization vector of a $\hat{y}$-directed dipole.

In the present work which is valid for every E- and H-plane feed patterns,

only the ones described by Eqs. 2.3 and 2.4 will be considered. For the sake of easiness, these two patterns will be written in a compact form as

$$\bar{E}_f(\rho,\theta,\phi) = A\,\frac{e^{-jk\rho}}{\rho}\sqrt{G_f(\theta)}\,\left(u_\theta \sin\phi\,\hat{\theta} + \cos\phi\,\hat{\phi}\right) \tag{2.5}$$

where

$$u_\theta = \begin{cases} \cos\theta & \text{for dipole feed} \\ 1 & \text{for Huygens source feed} \end{cases} \tag{2.6}$$

The feed patterns considered in this work are the $\cos^n\theta$ patterns thoroughly studied in the literature [15];

$$G_f(\theta) = \begin{cases} 2(n+1)\cos^n\theta & \theta \leqslant \pi/2 \\ 0 & \theta \geqslant \pi/2 \end{cases} \tag{2.7}$$

where n is a positive integer (n = 1, 2, 3, ...) and the feed pattern yielding uniform field distribution on the aperture plane, namely

$$G_f(\theta) = \begin{cases} \cot^2\frac{\alpha}{2} \Big/ \cos^4\frac{\theta}{2} & \theta < \alpha \\ 0 & \theta > \alpha \end{cases} \tag{2.8}$$

At the stationary points $Q_{\pm}$, which will come into picture in the following chapters, the incident electric field is simply; at $Q_+(\rho_o,\alpha,\phi)$

$$\bar{E}^{i1} = \bar{E}_f(\rho_o,\alpha,\phi) = A\,\frac{e^{-jk\rho_o}}{\rho_o}\sqrt{G_f(\alpha)}\,\left(u_\alpha \sin\phi\,\hat{\theta} + \cos\phi\,\hat{\phi}\right) \tag{2.9}$$

and at $Q_-(\rho_o,\alpha,\phi+\pi)$

$$\bar{E}^{i2} = \bar{E}_f(\rho_o,\alpha,\phi+\pi) = -\bar{E}^{i1} \tag{2.10}$$

where

$$u_\alpha = u_\theta\Big|_{\theta=\alpha} \tag{2.11}$$

2.2. Direct radiation from feed

The feed which is located at F, radiates directly into the free space as well as furnishing the paraboloid surface with incident electromagnetic waves. In this case, the direct feed radiated electric field may be expressed as

(ignoring $A\frac{e^{-jkR}}{R}$)

$$\bar{E}_f(R,\Theta,\Phi) = \sqrt{G_f(\Theta)}\left(u_\Theta \sin\Phi\,\hat{\Theta} + \cos\Phi\,\hat{\Phi}\right) \qquad (2.12)$$

where

$$u_\Theta = u_\theta\Big|_{\theta=\Theta} \qquad (2.13)$$

The reader is invited to pay attention to distinguishing the source coordinates (ρ,θ,ϕ) from the observation point coordinates (R,Θ,Φ).

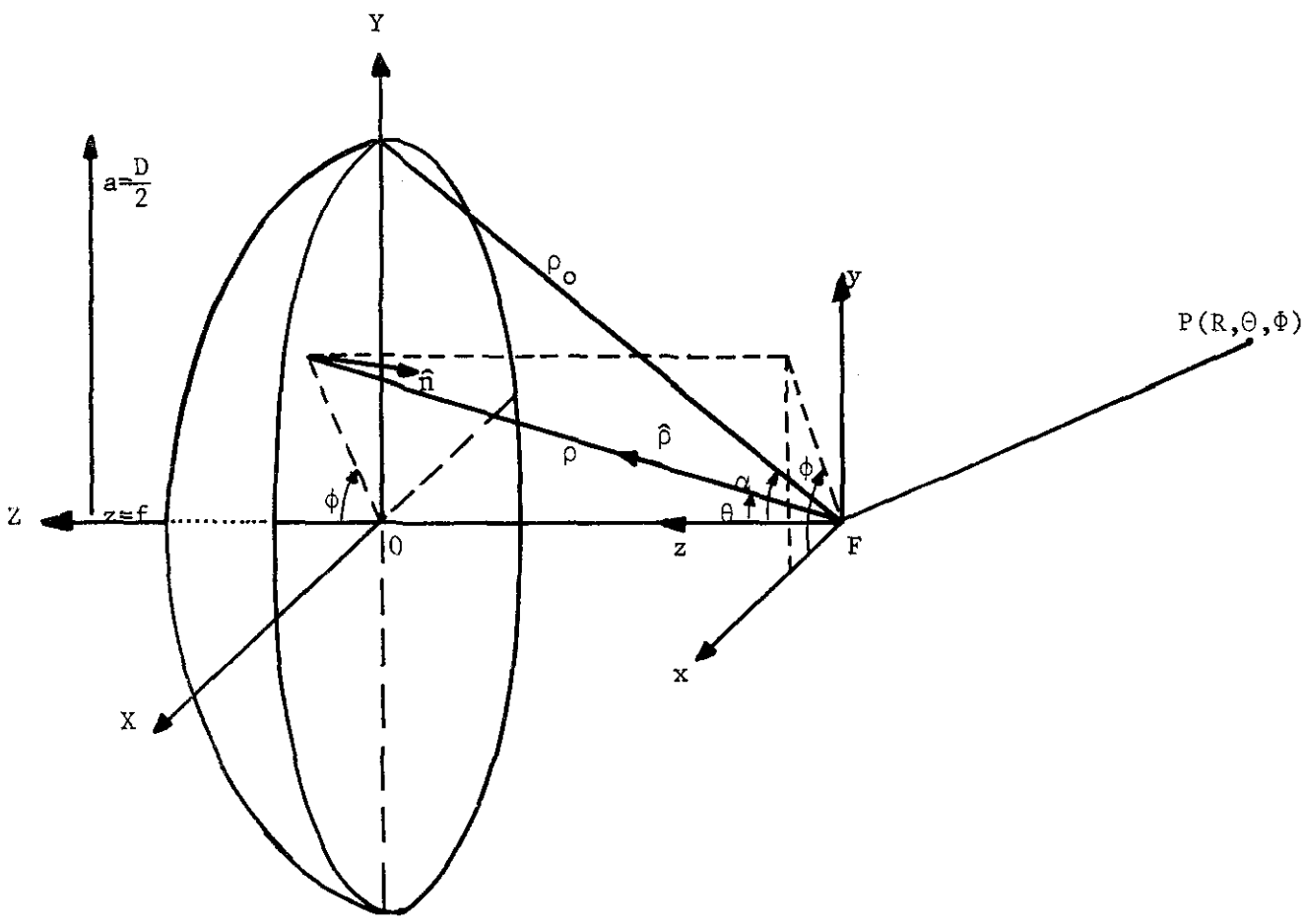

Fig. 2.1 Geometry of a focus-fed paraboloid.

3. GTD Analysis of radiation from paraboloid

3.1. Introduction

Let us consider a paraboloidal reflector, of radius a, whose edge lying in the XY-plane as shown in Fig. 3.1. Let the focus of the paraboloid be at F, the origion of (x,y,z) coordinate system. 2α is the subtended angle by the paraboloid. As in Fig. 2.1.1 (ρ,θ,ϕ) and (R,Θ,Φ) respectively denote the source and far-field coordinates.

According to the extension of Fermat's principle by Keller, at high frequencies $(2a/\lambda >> 1)$, the major contribution to the radiated field at $P(R,\Theta,\Phi)$ comes from two stationary edge points $Q_+(\rho_o,\alpha,\Phi)$ and $Q_-(\rho_o,\alpha,\Phi+\pi)$, the reference being (ρ,θ,ϕ) coordinate system. These two points $(Q\pm)$ are located at the intersection of the paraboloid edge with the plane passing through FOP (Fig. 3.1). As P approaches to $\pm$ z-axis, the plane defined by FOP degenerates to a line and consequently the contribution of the stationary edge points of the scattered field begin to loose their dominance and other points begin to contribute considerably as well; at the rear caustic direction $(\Theta=0)$, all the points on the paraboloid edge diffract with equal intensity, while for axial caustic field $(\Theta=\pi)$, scattering from the paraboloidal surface cannot any more be reduced to diffraction from the edge and the contribution of each point on the surface should be taken into account by integration.

For these reasons, GTD fails to estimate high frequency scattering from the paraboloid in the neighborhood of rear and axial caustics and these fields are calculated by equivalent edge cirrents method ([12] to [14]), which consists of integrating the diffracted field along the reflector edge, and physical optics integration ([15] to [17]) respectively.

The rays contributing to far-field radiation, for first order diffraction to which we confine the analysis, follow three paths, namely FQ_+P, FQ_-P and FP which stands for the direct feed radiation. Since R >> OF and due to the fact that all the contributing rays lie in the same plane, from Fig. 3.1 it can easily be observed that

$$\hat{S}_\pm \approx \hat{R} \tag{3.1}$$

$$S_\pm \approx R \qquad \text{for amplitude} \tag{3.2}$$

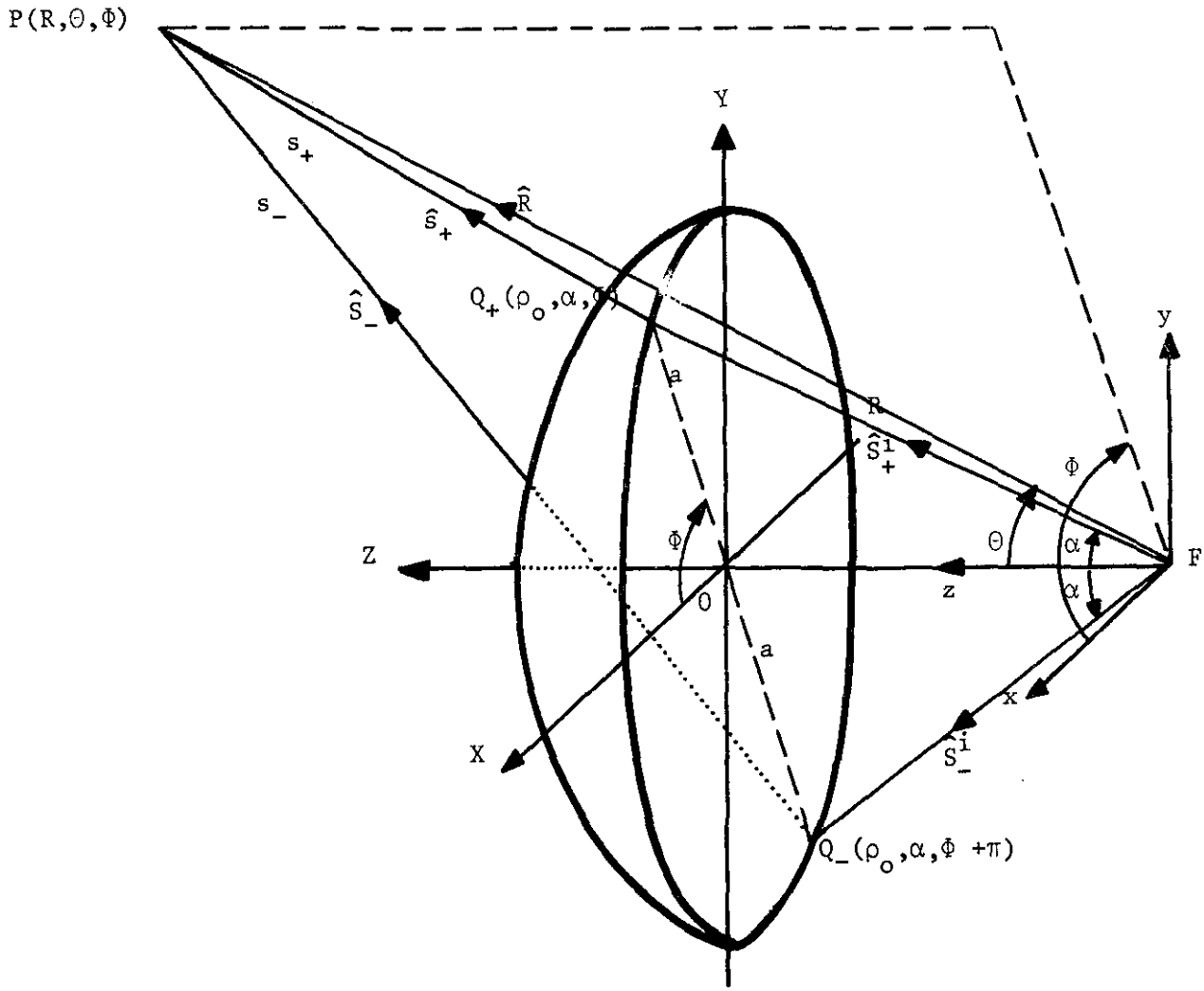

Fig. 3.1. Geometry of diffracted rays.

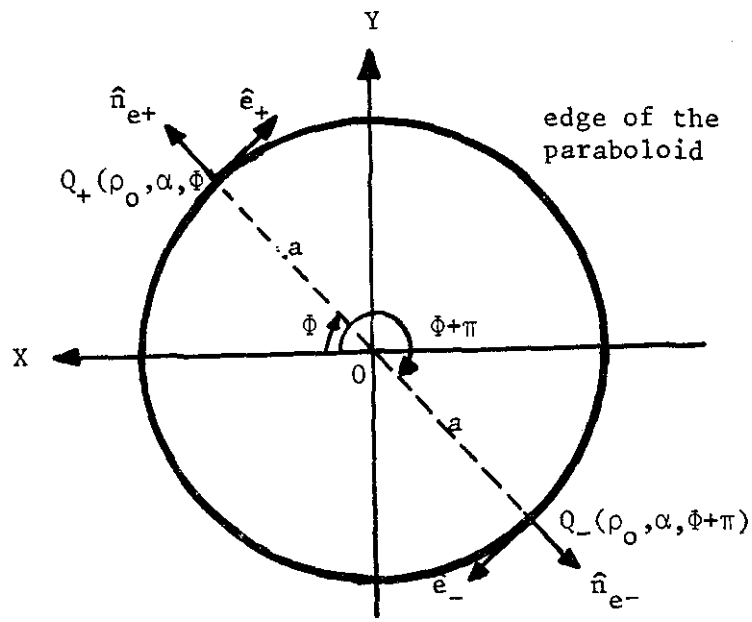

Fig. 3.2. Plane passing through the edge of the paraboloid.

$$s_{\pm} \approx R - \rho_0 \cos(\alpha \mp \Theta) \qquad \text{for phase} \qquad (3.3)$$

where $\hat{s}_{\pm}$ are the unit vectors along the diffracted rays from $Q_{\pm}$. On the other hand, $\hat{e}_{\pm}$ is the unit tangent vector at $Q_{\pm}$ and $\hat{n}e_{\pm}$, unit vector in the direction of $\overrightarrow{OQ_{\pm}}$ (Fig. 3.2). Radius of curvature of the paraboloid edge which describes a circle in XY plane is equal to the radius a at every Φ-plane. Thus, from Figs. 3.1 and 3.2, it is easy to write

$$\hat{n}e_{\pm} \cdot \hat{s}^i_{\pm} = \sin\alpha \qquad (3.4)$$

$$\hat{n}e_{\pm} \cdot \hat{s}_{\pm} = \pm \sin\Theta \qquad (3.5)$$

$$\rho^i_e = \rho_0 \qquad (3.6)$$

$$\kappa = a \qquad (3.7)$$

Inserting Eqs. 3.4 to 3.7 into Eq. A-3 yields the caustic distances

$$\rho_{c\pm} = \pm \rho_0 \frac{\sin\alpha}{\sin\Theta} \qquad (3.8)$$

From Eqs. A-5, A-6 and 3.8

$$L^i_{\pm} = |\rho_{c\pm}|_{SB} = \rho_0 \qquad (3.9)$$

and

$$L^r_{\pm} = \rho_{c\pm}\big|_{RB} \longrightarrow \infty \qquad (3.10)$$

3.2 Diffracted fields

3.2.1. Diffraction at Q_+ (See Fig. 3.3)

From Fig. 3.3, it is readily found that

$$\gamma^+_i = \frac{\pi - \alpha}{2} \qquad (3.11\ a)$$

$$\gamma^+_d = \frac{\alpha + 3\pi}{2} - \Theta \qquad (3.11\ b)$$

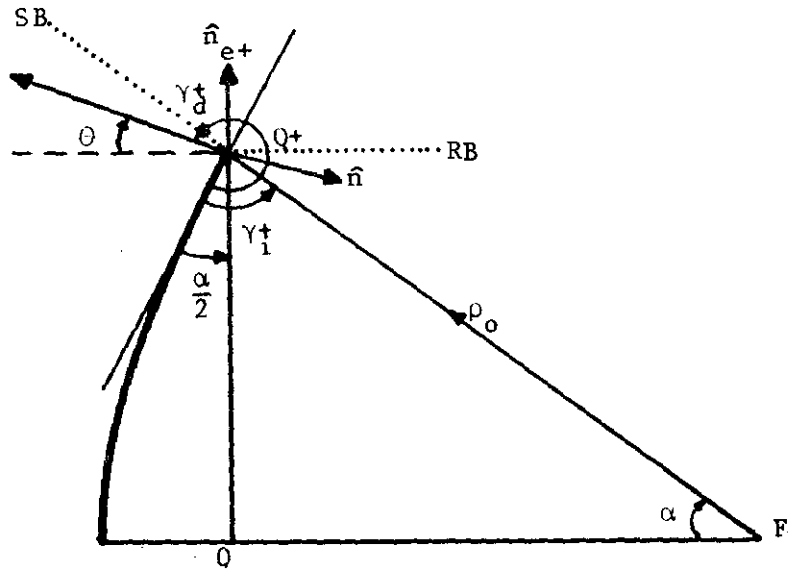

Fig. 3.3. Geometry of incident and diffracted rays at Q_+.

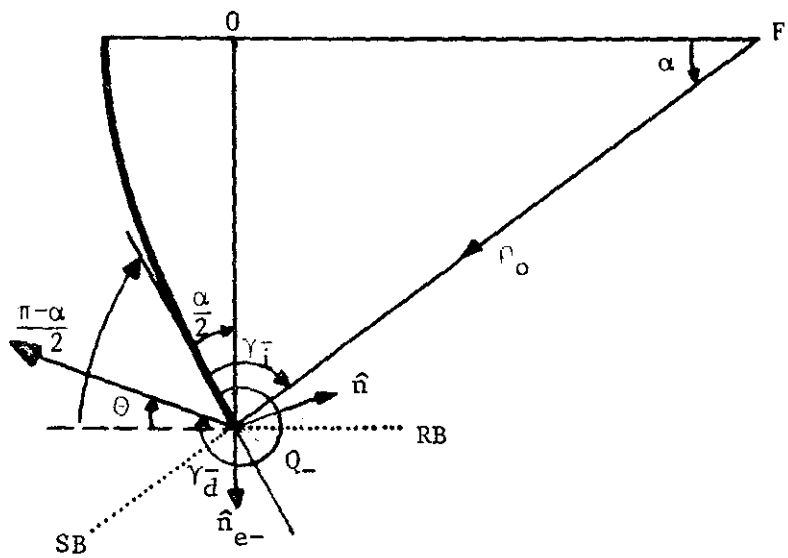

Fig. 3.4 Geometry of incident and diffracted rays at Q_-.

Substituting Eqs. 3.9 to 3.11 into A-4, we get

$$D_{h\atop s}^{+} = \frac{e^{-j\frac{\pi}{4}}}{2\sqrt{2\pi k}}\left[\frac{F(\omega_+ e^{j\frac{\pi}{4}})}{\sin\frac{\alpha-\theta}{2}} \pm \frac{1}{\cos\frac{\theta}{2}}\right] \tag{3.12}$$

where

$$\omega_\pm = \sqrt{2k\rho_o}\ \left|\sin\frac{\alpha \mp \theta}{2}\right| \tag{3.13}$$

Note that the transition function at reflection boundary is equal to unity because of Eqs. 3.10, A-7 and A-10.

Finally, Eq. A-1 reduces to (from Eqs. 2.9 and 3.1 to 3.12)

$$\left.\begin{matrix} E_\theta^+ \\ E_\phi^+ \end{matrix}\right\} = \frac{1}{2}\sqrt{\frac{G_f(\alpha)\sin\alpha}{2\pi k\rho_o \sin\theta}}\left\{\frac{F(\omega_+ e^{j\frac{\pi}{4}})}{\sin\frac{\alpha-\theta}{2}} \pm \frac{1}{\cos\frac{\theta}{2}}\right\}\left\{\begin{matrix} U_\alpha \sin\phi \\ \cos\phi \end{matrix}\right\} e^{-j\left(2k\rho_o \sin^2\frac{\alpha-\theta}{2} + \frac{\pi}{4}\right)} \tag{3.14}$$

where, from Eq. A-2,

$$\left.\begin{matrix} E_\theta^+ \\ E_\phi^+ \end{matrix}\right\} = \left\{\begin{matrix} E_\perp^+ \\ E_{\parallel}^+ \end{matrix}\right\} \tag{3.15}$$

and $A\,\frac{e^{-jkR}}{R}$ factor is ignored.

3.2.2. Diffraction at Q_- (See Fig. 3.4)

Proceeding similarly as in the previous section, we easily find

$$\gamma_i^- = \frac{\pi-\alpha}{2} \tag{3.16 a}$$

$$\gamma_d^- = \left\{\begin{matrix} \theta + \frac{\alpha+3\pi}{2} & \theta < \frac{\pi-\alpha}{2} \\ \theta + \frac{\alpha-\pi}{2} & \theta > \frac{\pi-\alpha}{2} \end{matrix}\right\} \tag{3.16 b}$$

From Eq. A-4, we find the diffraction coefficient at Q_-

$$\bar{D}_{\substack{h\\s}} = \frac{-\varepsilon_o e^{-j\frac{\pi}{4}}}{2\sqrt{2\pi k}} \left[\frac{F(\omega_- e^{j\frac{\pi}{4}})}{\sin\frac{\alpha+\theta}{2}} \pm \frac{1}{\cos\frac{\theta}{2}} \right] \tag{3.17}$$

where ω_- is defined by Eq. 3.13 and

$$\varepsilon_o = \begin{cases} -1 & \theta < \frac{\pi-\alpha}{2} \\ 0 & \frac{\pi-\alpha}{2} < \theta < \frac{\pi}{2} \\ 1 & \theta > \pi/2 \end{cases} \tag{3.18}$$

Note that the transition function at the reflection boundary is equal to unity by virtue of Eqs. 3.10, A-7 and A-10. ε_o is equal to zero in the region where the diffracted field at Q_- is shadowed by the paraboloidal reflector. Substitution of Eqs. 2.10, 3.1 to 3.3, 3.8 to 3.10, 3.16 and 3.17 into A-1 yields the singly diffracted field at Q_-

$$\begin{Bmatrix} \bar{E}_\theta \\ \bar{E}_\phi \end{Bmatrix} = \frac{\varepsilon_o}{2}\sqrt{\frac{G_f(\alpha)\sin\alpha}{2\pi k\rho_o \sin\theta}} \left\{ \frac{F(\omega_- e^{j\frac{\pi}{4}})}{\sin\frac{\alpha+\theta}{2}} \pm \frac{1}{\cos\frac{\theta}{2}} \right\} \begin{Bmatrix} u_\alpha \sin\Phi \\ \cos\Phi \end{Bmatrix} e^{-j\left(2k\rho_o \sin^2\frac{\alpha+\theta}{2} - \frac{\pi}{4}\right)} \tag{3.19}$$

where, from Eq. A-2,

$$\begin{Bmatrix} \bar{E}_\theta \\ \bar{E}_\phi \end{Bmatrix} = \begin{Bmatrix} \bar{E}_\perp \\ \bar{E}_\parallel \end{Bmatrix} \tag{3.20}$$

3.3. Total radiated field

Total radiated field ($\bar{E}^t$) at $P(R,\Theta,\Phi)$ (Fig. 3.5) is the sum of two singly diffracted fields with the direct feed radiation wherever observable. From Eqs. 2.12, 3.14 and 3.19 we get

$$\left.\begin{matrix} E_\theta^t \\ E_\phi^t \end{matrix}\right\} = \frac{1}{2}\sqrt{\frac{G_f(\alpha)\sin\alpha}{2\pi k\rho_o \sin\theta}}\left[\left\{\frac{F(\omega_+ e^{j\frac{\pi}{4}})}{\sin\frac{\alpha-\theta}{2}} \pm \frac{1}{\cos\frac{\theta}{2}}\right\} e^{-j\left(2k\rho_o \sin^2\frac{\alpha-\theta}{2}+\frac{\pi}{4}\right)} + \right.$$

$$\left. \varepsilon_o\left\{\frac{F(\omega_- e^{j\frac{\pi}{4}})}{\sin\frac{\alpha+\theta}{2}} \pm \frac{1}{\cos\frac{\theta}{2}}\right\} e^{-j\left(2k\rho_o \sin^2\frac{\alpha+\theta}{2}-\frac{\pi}{4}\right)}\right]\begin{bmatrix} u_\theta \sin\phi \\ \cos\phi \end{bmatrix} + \sqrt{G_f(\theta)}\begin{bmatrix} u_\theta \sin\phi \\ \cos\phi \end{bmatrix} U[(\theta-\alpha)(\tfrac{\pi}{2}-\theta)] \quad (3.21)$$

where the Heaviside unit step function U(z) = 1 or 0 for z > 0 and z < 0 respectively.

It is a known fact that E- and H-plane radiated fields from a paraboloid tend to have equal amplitudes as the observation point approaches forward and rear axial directions. Eq. 3.21 can be shown to satisfy this condition approximately in the neighborhood of the former but not for the latter. For this reason, GTD is expected to fail in predicting the backward radiation accurately enough.

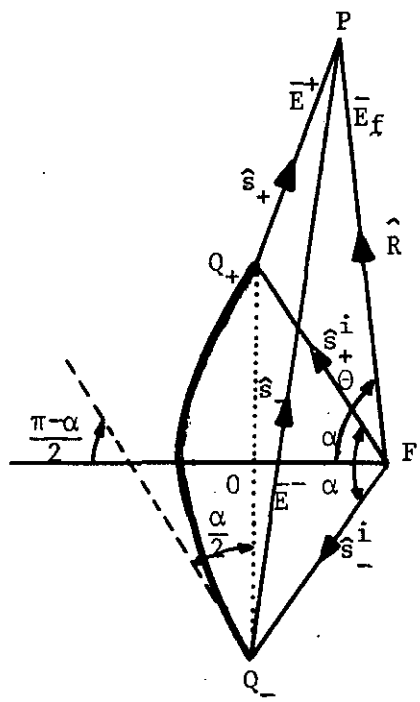

Fig. 3.5 Calculation of the total radiated field.

4. Physical optics analysis of radiation from paraboloid.

4.1. Problem formulation

Scattered far-field from a paraboloid, whose geometry is shown in Fig. 2.1, is given by [17]

$$\bar{E}(R,\Theta,\Phi) = \frac{-jk\eta}{4\pi}\frac{e^{-jkR}}{R}\iint_S \left[\bar{J}_s - (\bar{J}_s\cdot\hat{R})\hat{R}\right] e^{jk\rho\hat{\rho}\cdot\hat{R}}\, dS \tag{4.1}$$

where $\eta = 120\pi$ is the free space intrinsic wave impedance and $k = 2\pi/\lambda$ (λ = wavelength). From the geometry of a paraboloid, it is known that

$$\rho = \frac{2f}{1+\cos\theta} = f\sec^2\frac{\theta}{2} \tag{4.2}$$

where f denotes the focal distance (Fig. 2.1) and the surface element dS is

$$dS = 2\rho^2 \sin\frac{\theta}{2}\, d\theta\, d\phi \tag{4.3}$$

If the paraboloid is assumed to be at the far-field of the feed located at F (Fig. 2.1), the incident electromagnetic fields on the paraboloidal surface ($\bar{E}_i$, $\bar{H}_i$) satisfy the relation

$$\eta\bar{H}_i = \hat{\rho}\times\bar{E}_i \tag{4.4}$$

Paraboloidal surface current density $\bar{J}_s$ is given by geometrical optics approximation

$$\bar{J}_s = \begin{cases} 2(\hat{n}\times\bar{H}_i) & \text{illuminated surface} \\ 0 & \text{shaded surface} \end{cases} \tag{4.5}$$

where $\hat{n}$, given by

$$\hat{n} = -\cos\frac{\theta}{2}\,\hat{\rho} + \sin\frac{\theta}{2}\,\hat{\theta}\ , \tag{4.6}$$

is the outward unit normal vector on the surface. Incident electric field vector considered is, from Eq. 2.5,

$$\bar{E}_i = A\sqrt{G_f(\theta)}\,\frac{e^{-jk\rho}}{\rho}\left(u_\theta \sin\phi\,\hat{\theta} + \cos\phi\,\hat{\phi}\right) \tag{4.7}$$

where A, $G_f(\theta)$ and u_θ are defined in Chap. 2.
Substitution of Eqs. 4.4, 4.6 and 4.7 into 4.5 yields

$$\bar{J}_s = \begin{cases} \frac{2}{\eta} A\sqrt{G_f(\theta)}\,\frac{e^{-jk\rho}}{\rho}\cos\frac{\theta}{2}\left[u_\theta \tan\frac{\theta}{2}\sin\phi\,\hat{\rho} + u_\theta \sin\phi\,\hat{\theta} + \cos\phi\,\hat{\phi}\right] & \text{illuminated surface} \\ 0 & \text{shaded surface} \end{cases} \tag{4.8a}$$

which, in rectangular coordinates, reduces to

$$\bar{J}_s = \begin{cases} \frac{2}{\eta} A\sqrt{G_f(\theta)}\,\frac{e^{-jk\rho}}{\rho}\cos\frac{\theta}{2}\left[(u_\theta - 1)\sin\phi\cos\phi\,\hat{x} + \left\{1 + (u_\theta - 1)\sin^2\phi\right\}\hat{y} - u_\theta \tan\frac{\theta}{2}\sin\phi\,\hat{z}\right] & \text{illuminated surface} \\ 0 & \text{shaded surface} \end{cases} \tag{4.8b}$$

The above formula shows that if the feed is a Huygens source ($u_\theta = 1$), the current induced on the reflector surface has no cross-polar component ($\hat{x}$-component).
Decomposing $\bar{J}_s$ into its $\hat{\Theta}$-and $\hat{\Phi}$-components using Appendix B, one easily gets

$$\bar{J}_s \cdot \hat{\Theta} = \begin{cases} \frac{2}{\eta} A\sqrt{G_f(\theta)}\,\frac{e^{-jk\rho}}{\rho}\cos\frac{\theta}{2}\left[\cos\Theta\left\{\sin\Phi + (u_\theta - 1)\sin\phi\cos(\Phi - \phi)\right\} + \sin\Theta\, u_\theta \tan\frac{\theta}{2}\sin\phi\right] & \text{illuminated surface} \\ 0 & \text{shaded surface} \end{cases} \tag{4.9a}$$

and

$$\bar{J}_s \cdot \hat{\Phi} = \begin{cases} \frac{2}{\eta} A\sqrt{G_f(\theta)}\,\frac{e^{-jk\rho}}{\rho}\cos\frac{\theta}{2}\left[\cos\Phi - (u_\theta - 1)\sin\phi\sin(\Phi - \phi)\right] & \text{illuminated surface} \\ 0 & \text{shaded surface} \end{cases} \tag{4.9b}$$

With the help of Eq. 4.9, the integration over the whole reflector surface reduces to that over the illuminated surface only. Decomposing its $\hat{\Theta}$ and $\hat{\Phi}$ components, scattered field may be written as

$$\left.\begin{matrix} E_\theta \\ E_\phi \end{matrix}\right\} = \int_0^{\alpha} \int_0^{2\pi} \left\{\begin{matrix} f_\theta(\theta,\phi) \\ f_{\bar\phi}(\theta,\phi) \end{matrix}\right\} e^{-j\psi(\theta,\phi)} \, d\phi \, d\theta \tag{4.10}$$

where

$$\left.\begin{matrix} f_\theta(\theta,\phi) \\ f_{\bar\phi}(\theta,\phi) \end{matrix}\right\} \approx \frac{-j k\rho \sin\theta}{2\pi} \sqrt{G_f(\theta)} \left\{\begin{matrix} \cos\Theta\left\{\sin\bar\Phi + (u_\theta - 1)\sin\phi\cos(\bar\Phi - \phi)\right\} + \sin\Theta\, u_\theta \tan\frac{\theta}{2}\sin\phi \\ \cos\bar\Phi - (u_\theta - 1)\sin\phi\sin(\bar\Phi - \phi) \end{matrix}\right. \tag{4.11}$$

and, utilizing Appendix B,

$$\psi(\theta,\phi) = k\rho(1 - \hat\rho\cdot\hat R) = k\rho\left[1 - \cos\theta\cos\Theta - \sin\theta\sin\Theta\cos(\bar\Phi - \phi)\right] \tag{4.12}$$

Eq. 4.10 may also be written as

$$\left.\begin{matrix} E_\theta \\ E_\phi \end{matrix}\right\} = -j \int_0^{\alpha} k\rho\sin\theta \sqrt{G_f(\theta)}\; e^{-jk\rho(1-\cos\theta\cos\Theta)} \, I \, d\theta \tag{4.13}$$

where

$$I = \left\{\begin{matrix} \cos\Theta\sin\bar\Phi \\ \cos\bar\Phi \end{matrix}\right\} \frac{1}{2\pi} \int_0^{2\pi} e^{j\beta\cos(\bar\Phi - \phi)} \, d\phi + \left\{\begin{matrix} \sin\Theta \\ 0 \end{matrix}\right\} \frac{u_\theta \tan\frac{\theta}{2}}{2\pi} \int_0^{2\pi} \sin\phi \; e^{j\beta\cos(\bar\Phi - \phi)} \, d\phi$$

$$+ \left\{\begin{matrix} \cos\Theta \\ -1 \end{matrix}\right\} \frac{u_\theta - 1}{2\pi} \int_0^{2\pi} \sin\phi \left\{\begin{matrix} \cos(\bar\Phi - \phi) \\ \sin(\bar\Phi - \phi) \end{matrix}\right\} e^{j\beta\cos(\bar\Phi - \phi)} \, d\phi \tag{4.14}$$

From Eqs. D-2, D-7 and D-8, I reduces to

$$I = \left\{\begin{matrix} \cos\Theta\sin\bar\Phi \\ \cos\bar\Phi \end{matrix}\right\} J_0(\beta) + \left\{\begin{matrix} \sin\Theta\sin\bar\Phi \\ 0 \end{matrix}\right\} j u_\theta \tan\frac{\theta}{2} J_1(\beta) + \left\{\begin{matrix} \cos\Theta\sin\bar\Phi \\ \cos\bar\Phi \end{matrix}\right\} \frac{u_\theta - 1}{2}\left\{J_0(\beta) \mp J_2(\beta)\right\} \tag{4.15}$$

where β is defined by

$$\beta = k\rho\sin\theta\sin\Theta \tag{4.16}$$

Inserting Eq. 4.15 into 4.13, we get

$$\left.\begin{matrix} E_\theta \\ E_\phi \end{matrix}\right\} = \left\{\begin{matrix} \cos\Theta \sin\Phi \\ \cos\Phi \end{matrix}\right\} e^{-j\frac{\pi}{2}} \int_0^\alpha k\rho \sin\theta \sqrt{G_f(\theta)}\, J_0(\beta)\, e^{-jk\rho(1-\cos\theta\cos\Theta)}\, d\theta$$

$$+ \left\{\begin{matrix} \cos\Theta \sin\Phi \\ \cos\Phi \end{matrix}\right\} e^{-j\frac{\pi}{2}} \int_0^\alpha k\rho \sin\theta \sqrt{G_f(\theta)} \left[J_0(\beta) \mp J_2(\beta)\right] \frac{u_\theta - 1}{2}\, e^{-jk\rho(1-\cos\theta\cos\Theta)}\, d\theta$$

$$+ \left\{\begin{matrix} \sin\Theta \sin\Phi \\ 0 \end{matrix}\right\} \int_0^\alpha k\rho \sin\theta \sqrt{G_f(\theta)}\, u_\theta \tan\frac{\theta}{2}\, J_1(\beta)\, e^{-jk\rho(1-\cos\theta\cos\Theta)}\, d\theta \qquad (4.17a)$$

From Eqs. 4.8 to 4.15 it is evident that the first (second) integral term of Eq. 4.17a represents the radiation from $\hat{y}$-polarised ($\hat{x}$-polarised) surface currents while the last integral accounts for radiation from $\hat{z}$-directed currents. For Huygens source feeding ($u_\theta = 1$) the second integral term vanishes. Further in the vicinity of broadside direction, radiating aperture looks like a $\hat{y}$-directed dipole.

For future use, the preceeding equation will be written in a more compact form as

$$\left.\begin{matrix} E_\theta \\ E_\phi \end{matrix}\right\} = \left\{\begin{matrix} \cos\Theta \sin\Phi \\ \cos\Phi \end{matrix}\right\} e^{-j\frac{\pi}{2}} \int_0^\alpha k\rho \sin\theta \sqrt{G_f(\theta)} \left[J_0(\beta)\, \frac{u_\theta + 1}{2} \mp J_2(\beta)\, \frac{u_\theta - 1}{2}\right] e^{-jk\rho(1-\cos\theta\cos\Theta)}\, d\theta$$

$$+ \left\{\begin{matrix} \sin\Theta \sin\Phi \\ 0 \end{matrix}\right\} \int_0^\alpha k\rho \sin\theta \sqrt{G_f(\theta)}\, u_\theta \tan\frac{\theta}{2}\, J_1(\beta)\, e^{-jk\rho(1-\cos\theta\cos\Theta)}\, d\theta \qquad (4.17b)$$

It is interesting to note that the first part of the Eq. 4.17b represents the far field radiation from a circular aperture of radius a over which the electric field vector is polarised on the aperture plane. Further, if u_θ is replaced by unity, then it reduces to the radiation from a circular aperture with $\hat{y}$-polarised electric field distribution on it. This method of calculating the far field of a paraboloid, which is valid only in the close vicinity of forward and backward axial directions, is known as the aperture field theory [15].

It is difficult to perform the integrations analytically in the above equation. Besides, since the Bessel functions vary rapidly with β when the observation point is not near to rear or forward axial directions, Eq. 4.17b, having a rapidly varying kernel, is not suitable for asymptotic evaluation ([19] to [22]).

4.2. Asymptotic physical optics (APO)

In the pervious section, we observed that Eq. 4.17b has a large parameter in its phase term and a rapidly varying kernel. For this reason, it can not be evaluated asymptotically.

We know that for large values of β, the Bessel functions in Eq. 4.17b can asymptotically be written as [23]

$$J_m(\beta) \sim \sqrt{\frac{2}{\pi\beta}}\cos\left(\beta - \frac{m\pi}{2} - \frac{\pi}{4}\right)$$

$$= \frac{1}{\sqrt{2\pi\beta}}\left[e^{j\left(\beta - \frac{\pi}{4} - \frac{m\pi}{2}\right)} + e^{-j\left(\beta - \frac{\pi}{4} - \frac{m\pi}{2}\right)}\right] \tag{4.18}$$

Eq. 4.18 can readily be obtained by expanding Eq. D-1 asymptotically. From this expansion one may easily observe that the first term of the last part of Eq. 4.18 is equal to the contribution of the plus stationary point

$$\Phi_+ = \Phi \tag{E-7}$$

and the second term is the contribution of the minus stationary point defined by

$$\Phi_- = \Phi + \pi \tag{E-8}$$

It is of importance to note that the large values of β corresponds to the values of Θ sufficiently far from the forward and rear axial directions.

Substituting Eq. 4.18 into Eq. 4.17b and rearranging, one may write the scattered field as a sum of the two stationary points contributions

$$\begin{Bmatrix} E_\theta \\ E_\Phi \end{Bmatrix} = \begin{Bmatrix} E_\theta^+ \\ E_\Phi^+ \end{Bmatrix} + \begin{Bmatrix} E_\theta^- \\ E_\Phi^- \end{Bmatrix} \tag{4.19}$$

where

$$\begin{Bmatrix} E_\theta^\pm \\ E_\Phi^\pm \end{Bmatrix} = \int_0^\alpha \begin{Bmatrix} h_\theta(\theta,\phi_\pm) \\ h_\Phi(\theta,\phi_\pm) \end{Bmatrix} e^{-j\psi(\theta,\phi_\pm)}\, d\theta \tag{4.19a}$$

The new integral kernel is found, from Eqs. F-2 and C-4, as

$$\left.\begin{matrix} h_\Theta(\theta,\phi_\pm) \\ h_\Phi(\theta,\phi_\pm) \end{matrix}\right\} = \left\{\begin{matrix} f_\Theta(\theta,\phi_\pm) \\ f_\Phi(\theta,\phi_\pm) \end{matrix}\right\} \sqrt{\frac{2\pi}{|\psi_{\phi\phi}(\theta,\phi_\pm)|}}\; e^{\mp j\frac{\pi}{4}}$$

$$= -j \left\{\begin{matrix} u_\theta \sin\Phi \\ \cos\Phi \end{matrix}\right\} \left\{\begin{matrix} \cos(\Theta \mp \frac{\theta}{2}) \\ \cos\frac{\theta}{2} \\ 1 \end{matrix}\right\} \sqrt{\frac{G_f(\theta)\, k\rho\sin\theta}{2\pi \sin\Theta}}\; e^{\mp j\frac{\pi}{4}} \qquad (4.19b)$$

$$\psi(\theta,\phi_\pm) = 2k\rho \sin^2\frac{\theta \mp \Theta}{2} \qquad (E\text{-}9)$$

and

$$\psi_{\phi\phi}(\theta,\phi_\pm) = \pm k\rho \sin\theta \sin\Theta \qquad (E\text{-}10)$$

Comparison of Eqs. 4.19 and C-4 shows that Eq. 4.19a corresponds to the stationary phase evaluation of 4.10 with respect to ϕ where the contributions of the end-points, $\phi = 0, 2\pi$, identically cancel each other. From the above reasoning, it is easy to conclude that, away from the axial directions, the most significant contributions to the radiated field from a large paraboloid come from the points located at the intersection of paraboloid with the stationary planes (defined by $\phi_\pm$) lying at the same plane as the observation point. These points obviously satisfy Fermat's principle, i.e. they make Eq. 4.12 stationary. Since Eq. 4.19b varies slowly with θ and Eq. E-9 contains a positif large parameter, the requirements for an asymptotic evaluation are satisfied. For this reason, Eq. 4.19a can be evaluated asymptotically.

4.2.1. An asymptotic evaluation of Eq. 4.19a.

Eq. E-11 shows that the phase term in Eq. 4.19a has stationary points, given by

$$\theta_\pm = \pm\Theta \qquad (4.20)$$

which disappear from the integration interval ($0 \leqslant \theta \leqslant \alpha$) as the observation point swings across the shadow boundary. The most significant contributions to the integral equation 4.19a come from the stationary points, defined by Eq. 4.20, and from the end-points of the integration interval ($\theta = 0$ and α). Evaluation of

such an integral, where the stationary points uniformly approach the end-points, is explained in Appendix C.

Using Eq. C-6, Eq. 4.19a may be asymptotically written as

$$\left.\begin{matrix} E_\theta^\pm \\ E_\phi^\pm \end{matrix}\right\} = \left\{\begin{matrix} I_{e\theta}^\pm \\ I_{e\phi}^\pm \end{matrix}\right\} + \left\{\begin{matrix} I_{s\theta}^\pm \\ I_{s\phi}^\pm \end{matrix}\right\} W(s_\pm e^{j\frac{\pi}{4}}) \tag{4.21}$$

where the only end-point contribution is due to $\theta = \alpha$ since the kernel of Eq. 4.19a vanishes at the other end-point, $\theta = 0$. From Eq. C-5, the first order end-point contribution is

$$\left.\begin{matrix} I_{e\theta}^\pm \\ I_{e\phi}^\pm \end{matrix}\right\} = \frac{1}{2}\sqrt{\frac{G_f(\alpha)\sin\alpha}{2\pi k\rho_o \sin\theta}} \left\{\begin{matrix} U_\alpha \sin\Phi\, K_\theta^\pm \\ \cos\Phi \quad K_\phi^\pm \end{matrix}\right\} \frac{e^{-j\left(2k\rho_o \sin^2\frac{\alpha\mp\theta}{2} \pm \frac{\pi}{4}\right)}}{\sin\frac{\alpha\mp\theta}{2}} \tag{4.22}$$

and, from Eq. C-4, the first order stationary point contribution simply is

$$\left.\begin{matrix} I_{s\theta}^\pm \\ I_{s\phi}^\pm \end{matrix}\right\} = \mp \left\{\begin{matrix} U_\theta \sin\Phi \\ \cos\Phi \end{matrix}\right\} \sqrt{G_f(\theta)} \tag{4.23}$$

$$\left.\begin{matrix} K_\theta^\pm \\ K_\phi^\pm \end{matrix}\right\} = \left\{\begin{matrix} K_{k\theta}^\pm \\ K_{k\phi}^\pm \end{matrix}\right\} \frac{1}{K_e^\pm} = \left\{\begin{matrix} \cos(\theta \mp \frac{\alpha}{2}) \\ \cos\frac{\alpha}{2} \end{matrix}\right\} \frac{1}{\cos\frac{\theta}{2}} \tag{4.24}$$

where $K_e^\pm$, defined by Eq. E-23, results from the phase term (Eq. E-20) while $(K_{k\theta}^\pm, K_{k\phi}^\pm)$ is due to the kernel given by Eq. F-4. Besides, $W(s_\pm e^{j\pi/4})$ is defined by Eq. C-10 with an argument

$$s_\pm = \pm\sqrt{2k\rho_o}\, \sin\frac{\alpha\mp\theta}{2} \tag{4.25}$$

which is determined by Eq. C-13.

Note that as the observation point approaches the shadow boundary, second term of W function (Eq. C-10), multiplied by the stationary point contribution, identically cancels the end-point contribution thus yielding a far-field equal

to minus half the incident field as expected. When the observation point is considerably far from the shadow boundary, W function reduces to unity or zero in the shadow and illuminated regions respectively.

4.2.2. A second asymptotic evaluation of Eq. 4.19a.

Since the kernel of Eq. 4.19a is a slowly varying function of θ, the significant contribution of this integral comes from the neighborhood of the stationary points $\theta_{\pm} = \pm\Theta$ and from that of the end-point $\theta = \alpha$. Expanding the phase function around these points and assuming that the kernel, in these neighborhoods, varies slowly, Eq. 4.19a can be easily evaluated by asymptotic techniques.

a) Stationary point contribution

Expanding the phase function around the stationary points (Eq. 4.20), one gets from Eqs. E-14 to E-17 by limiting the expansion at first two derivatives

$$\Psi(\theta,\phi_{\pm}) \cong \frac{1}{2}\Psi_{\theta\theta}(\pm\Theta,\phi_{\pm})(\theta\mp\Theta)^2 = \frac{1}{2}\,k\rho(\Theta)\,(\theta\mp\Theta)^2 \tag{4.26}$$

In the neighborhood of stationary points, Eq. 4.19a is approximately

$$\left.\begin{matrix} E_{s\Theta}^{\pm} \\ E_{s\Phi}^{\pm} \end{matrix}\right\} = \left\{\begin{matrix} h_{\Theta}(\pm\Theta,\phi_{\pm}) \\ h_{\Phi}(\pm\Theta,\phi_{\pm}) \end{matrix}\right\} \int_0^{\alpha} e^{-j\frac{1}{2}k\rho(\Theta)(\theta\mp\Theta)^2}\, d\theta \tag{4.27}$$

which, from the definition of Q function (Eq. A-8), reduces to

$$\left.\begin{matrix} E_{s\Theta}^{\pm} \\ E_{s\Phi}^{\pm} \end{matrix}\right\} = \pm\left\{\begin{matrix} I_{s\Theta}^{\pm} \\ I_{s\Phi}^{\pm} \end{matrix}\right\} Q\left(\mp\sqrt{2k\rho(\Theta)}\,\frac{\alpha\mp\Theta}{2}\,e^{j\frac{\pi}{4}}\right) U(\alpha-\Theta) \tag{4.28}$$

b) End-point contribution

Expanding the phase function around the end-point $\theta = \alpha$ and limiting this expansion at first two derivatives, one easily gets

$$\Psi(\theta,\phi_{\pm}) \cong \Psi(\alpha,\phi_{\pm}) + \Psi_{\theta}(\alpha,\phi_{\pm})(\theta-\alpha) + \frac{1}{2}\Psi_{\theta\theta}(\alpha,\phi_{\pm})(\theta-\alpha)^2 \tag{4.29}$$

Proceeding similarly as in the case of stationary point evaluation, one obtains

$$\left.\begin{matrix} E^{\pm}_{e\theta} \\ E^{\pm}_{e\phi} \end{matrix}\right\} = \left\{\begin{matrix} h_\theta(\alpha,\phi_\pm) \\ h_\phi(\alpha,\phi_\pm) \end{matrix}\right\} e^{-j\psi(\alpha,\phi_\pm)} \int_0^\alpha e^{-j\left[\psi_\theta(\alpha,\phi_\pm)(\theta-\alpha)+\frac{1}{2}\psi_{\theta\theta}(\alpha,\phi_\pm)(\theta-\alpha)^2\right]} d\theta \qquad (4.30)$$

From Eq. G-5

$$\int_0^\alpha e^{-j\left[\psi_\theta(\alpha,\phi_\pm)(\theta-\alpha)+\frac{1}{2}\psi_{\theta\theta}(\alpha,\phi_\pm)(\theta-\alpha)^2\right]} d\theta = \frac{F\left(|d_\pm| e^{j\frac{\pi}{4}}\right)}{-j\psi_\theta(\alpha,\phi_\pm)} \qquad (G\text{-}5)$$

where

$$d_\pm = \frac{\psi_\theta(\alpha,\phi_\pm)}{\sqrt{2|\psi_{\theta\theta}(\alpha,\phi_\pm)|}} = \sqrt{\frac{2k\rho_0\left|\cos\frac{\theta}{2}\right|}{\left|2\cos\frac{\theta}{2}-\cos\left(\alpha\mp\frac{\theta}{2}\right)\right|}}\ \sin\frac{\alpha\mp\theta}{2} \qquad (G\text{-}4)$$

Insertion of Eq. G-5 into 4.30 yields

$$\left.\begin{matrix} E^{\pm}_{e\theta} \\ E^{\pm}_{e\phi} \end{matrix}\right\} = \left\{\begin{matrix} I^{\pm}_{e\theta} \\ I^{\pm}_{e\phi} \end{matrix}\right\} F\left(|d_\pm| e^{j\frac{\pi}{4}}\right) \qquad (4.31)$$

where ($I^{\pm}_{e\theta}$, $I^{\pm}_{e\phi}$) is defined by Eq. 4.22.
The scattered field (Eq. 4.19a) is found by the summation of Eqs. 4.28 and 4.31

$$\left.\begin{matrix} E^{\pm}_{\theta} \\ E^{\pm}_{\phi} \end{matrix}\right\} = \left\{\begin{matrix} I^{\pm}_{e\theta} \\ I^{\pm}_{e\phi} \end{matrix}\right\} F\left(|d_\pm| e^{j\frac{\pi}{4}}\right) \pm \left\{\begin{matrix} I^{\pm}_{s\theta} \\ I^{\pm}_{s\phi} \end{matrix}\right\} Q\left(\mp\sqrt{2k\rho(\theta)}\ \frac{\alpha\mp\theta}{2}\ e^{j\frac{\pi}{4}}\right) U(\alpha-\theta) \qquad (4.32)$$

4.2.3. Total radiated field

Total radiated field from the paraboloidal reflector antenna system is equal to the addition of direct feed radiation (Eq. 2.12) and the total scattered field given by Eq. 4.21 or Eq. 4.32;

$$\begin{Bmatrix} E_\theta^t \\ E_\phi^t \end{Bmatrix} = \begin{Bmatrix} E_\theta^+ \\ E_\phi^+ \end{Bmatrix} + \begin{Bmatrix} E_\theta^- \\ E_\phi^- \end{Bmatrix} - \begin{Bmatrix} I_{s\theta}^+ \\ I_{s\phi}^+ \end{Bmatrix} U\left(\frac{\pi}{2}-\theta\right) \tag{4.33}$$

where the direct feed radiation is written in terms of the stationary point contribution.

If the asymptotic evaluation given by Eq. 4.21 is used, Eq. 4.33 is simply

$$\begin{Bmatrix} E_\theta^t \\ E_\phi^t \end{Bmatrix} = \begin{Bmatrix} I_{e\theta}^+ \\ I_{e\phi}^+ \end{Bmatrix} + \begin{Bmatrix} I_{e\theta}^- \\ I_{e\phi}^- \end{Bmatrix} - \begin{Bmatrix} I_{s\theta}^+ \\ I_{s\phi}^+ \end{Bmatrix} \left[W\left(|s+1|\, e^{\frac{j\pi}{4}}\right) + U(\theta-\alpha)\right] U\left(\frac{\pi}{2}-\theta\right) \tag{4.34}$$

where $W(s\_e^{j\pi/4}) = 0$ by virtue of Eqs. 4.25 and C-11.

If Eq. 4.32 is inserted into Eq. 4.33, one obtains

$$\begin{Bmatrix} E_\theta^t \\ E_\phi^t \end{Bmatrix} = \begin{Bmatrix} I_{e\theta}^+ \\ I_{e\phi}^+ \end{Bmatrix} F\left(|d+1|\, e^{\frac{j\pi}{4}}\right) + \begin{Bmatrix} I_{e\theta}^- \\ I_{e\phi}^- \end{Bmatrix} F\left(|d-1|\, e^{\frac{j\pi}{4}}\right) - \begin{Bmatrix} I_{s\theta}^+ \\ I_{s\phi}^+ \end{Bmatrix} U\left[(\theta-\alpha)\left(\frac{\pi}{2}-\theta\right)\right] \tag{4.35}$$

where $Q\left(\sqrt{2k\rho(\theta)}\ \left|\frac{\alpha\pm\theta}{2}\right|\ e^{j\pi/4}\right)$, which is approximately equal to zero except in the near vicinity of the shadow boundary, is considered to be zero.

4.3. Asymptotic physical optics theory of Rusch

Rusch in his asymptotic physical optics theory [8] applies the method described in section 4.2.2 directly to Eq. 4.10 instead of proceeding with Eq. 4.19a; but by virtue of the first part of Eq. 4.19b, they yield the same result. In addition to this, he performes the asymptotic evaluation in aperture plane and in cartesian coordinates.

Stationary point contribution of Rusch is equal to minus the geometrical optics term and in Eq. G-5, he takes the transition function as unity [8]. These respectively yield discontinuous and infinite fields at the shadow boundary. His theory has recently been extended by Knop [11] by introducing the transition functions in Eq. G-5. Knop's solution, with a transformation given by Table 4.1 yields a total field ([11] , Eq. 26)

Table 4.1
Transformation of Knop's variables

Knop [11]	Safak
θ	$\pi - \Theta$
ρ_D	ρ_o
θ_D	$\pi - \alpha$
$k(\rho_D - z_{sp}\cos\theta \mp a\sin\theta)$	$2k\rho_o \sin^2\frac{\alpha \mp \Theta}{2}$
$\sqrt{\frac{\pi}{2}}\lvert\omega^{\pm}\rvert = \sqrt{\frac{ka\sin\theta}{2}}\left\lvert 1 \mp \frac{\tan\frac{\theta}{2}}{\tan\frac{\theta_D}{2}}\right\rvert$	$\gamma^{\pm} = \sqrt{2k\lvert\rho_{c\pm}\rvert}\, K_e^{\pm}\left\lvert\sin\frac{\alpha \mp \Theta}{2}\right\rvert$
$-\left[\cos\theta \mp \frac{\sin\theta}{\tan\frac{\theta_D}{2}}\right]$	$K_{k\Theta} = \cos\Theta \pm \tan\frac{\alpha}{2}\sin\Theta$
$\left[C(\omega^{\pm}) - \frac{1}{2}\right] \mp j\left[S(\omega^{\pm}) - \frac{1}{2}\right]$	$-\sqrt{2}\, e^{\mp j\frac{\pi}{4}}\, Q(\gamma^{\pm} e^{\pm j\frac{\pi}{4}})$
$\varepsilon_o \frac{e^{-jk\rho}}{\rho}\begin{Bmatrix} A(\psi)\, e^{j\alpha(\psi)} & \cos\xi \\ B(\psi)\, e^{j\beta(\psi)} & \sin\xi \end{Bmatrix}$	$A\frac{e^{-jk\rho}}{\rho}\sqrt{G_f(\theta)}\begin{Bmatrix} u_\theta \sin\phi \\ \cos\phi \end{Bmatrix}$

$$\left.\begin{matrix} E_\theta^t \\ E_\phi^t \end{matrix}\right\} = \left\{\begin{matrix} I_{e\theta}^+ \\ I_{e\phi}^+ \end{matrix}\right\} F(\gamma^+ e^{j\frac{\pi}{4}}) + \left\{\begin{matrix} I_{e\theta}^- \\ I_{e\phi}^- \end{matrix}\right\} F(\gamma^- e^{-j\frac{\pi}{4}}) - \left\{\begin{matrix} I_{s\theta}^+ \\ I_{s\phi}^+ \end{matrix}\right\} U\left[\left(\tfrac{\pi}{2}-\theta\right)(\theta-\alpha)\right] \quad (4.36)$$

where

$$\gamma^\pm = \sqrt{2\,k|\rho_{c\pm}|}\;\; K_e^\pm \left|\sin\frac{\alpha \mp \theta}{2}\right| \quad (4.37)$$

and

$$K_e^\pm = \sec\frac{\alpha}{2}\cos\frac{\theta}{2} \quad (E\text{-}23)$$

$\rho_{c\pm}$ are the caustic distances at $\pm$ stationary points Eqs. 3.8

$$\rho_{c\pm} = \pm\rho_0\frac{\sin\alpha}{\sin\theta} \quad (4.38)$$

The difference between the arguments of the transition functions of Knop and those of section 4.2.2 may be attributed to the approximations made by Knop in evaluating Eq. G-5 [11].

Physical optics diffraction coefficients ([11], Eq. 33), with the aid of Table 4.1 may be written as*

$$\left.\begin{matrix} D_h^\pm \\ D_s^\pm \end{matrix}\right\} = \frac{\pm\, e^{-j\frac{\pi}{4}}}{2\sqrt{2\pi k}} \left\{\begin{matrix} K_\theta^\pm \\ K_\phi^\pm \end{matrix}\right\} \frac{F(\gamma^\pm\, e^{\pm j\frac{\pi}{4}})}{\sin\frac{\alpha \mp \theta}{2}} \quad (4.39)$$

* In [11 , Eq. 33] $\pm$ term in front of Eq. 4.39 is missing.

4.4. Comparison of GTD and PO diffraction coefficients

Physical optics diffraction coefficients from Eqs. 4.22 and 4.31 may easily be written as

$$\left.\begin{matrix} D_h^{\pm} \\ D_s^{\pm} \end{matrix}\right\} = \frac{\pm e^{-j\frac{\pi}{4}}}{2\sqrt{2\pi k}} \left\{\begin{matrix} K_\theta^{\pm} \\ K_\phi^{\pm} \end{matrix}\right\} \frac{F(|d_\pm| e^{j\frac{\pi}{4}})}{\sin\frac{\alpha \mp \theta}{2}} \tag{4.40}$$

where

$$\left.\begin{matrix} K_\theta^{\pm} \\ K_\phi^{\pm} \end{matrix}\right\} = \left\{\begin{matrix} \cos(\theta \mp \frac{\alpha}{2}) \\ \cos\frac{\alpha}{2} \end{matrix}\right\} \frac{1}{\cos\frac{\theta}{2}} \tag{4.24}$$

and

$$d_\pm = \sqrt{\frac{2k\rho_0 |\cos\frac{\theta}{2}|}{|2\cos\frac{\theta}{2} - \cos(\alpha \mp \frac{\theta}{2})|}} \quad \sin\frac{\alpha \mp \theta}{2} \tag{G-4}$$

Comparison of Eq. 4.40 with Eq. 4.39 shows that in Knop's PO diffraction coefficients $|d_\pm| e^{j\pi/4}$ is replaced by $\gamma_\pm e^{\pm j\frac{\pi}{4}}$ in the argument of transition functions.

GTD diffraction coefficients are from Eqs. 3.12 and 3.17

$$D_s^h = \frac{e^{-j\frac{\pi}{4}}}{2\sqrt{2\pi k}} \left[\frac{F(\omega_+ e^{j\frac{\pi}{4}})}{\sin\frac{\alpha-\theta}{2}} \pm \frac{1}{\cos\frac{\theta}{2}} \right] \tag{4.41a}$$

$$D_s^h = \frac{-\varepsilon_0 e^{-j\frac{\pi}{4}}}{2\sqrt{2\pi k}} \left[\frac{F(\omega_- e^{j\frac{\pi}{4}})}{\sin\frac{\alpha+\theta}{2}} \pm \frac{1}{\cos\frac{\theta}{2}} \right] \tag{4.41b}$$

where

$$\omega_\pm = \sqrt{2k\rho_0} \; |\sin\frac{\alpha \mp \theta}{2}| \tag{3.13}$$

and

$$\varepsilon_0 = \left\{\begin{matrix} -1 & \theta < \frac{\pi-\alpha}{2} \\ 0 & \frac{\pi-\alpha}{2} < \theta < \frac{\pi}{2} \\ 1 & \theta > \frac{\pi}{2} \end{matrix}\right\} \tag{3.18}$$

It is easy to observe that in the vicinity of the shadow boundary ($\Theta = \pm\alpha$) Eq. 4.40 may approximately be written as

$$\left.\begin{matrix} D_h^{\pm} \\ D_s^{\pm} \end{matrix}\right\}_{SB} \sim \frac{\pm\, e^{-j\frac{\pi}{4}}}{2\sqrt{2\pi k}}\; \frac{F(\omega_{\pm}\, e^{j\frac{\pi}{4}})}{\sin\frac{\alpha \mp \Theta}{2}} \left\{\begin{matrix} 1 \\ 1 \end{matrix}\right\} \tag{4.42}$$

since

$$\left.\begin{matrix} K_{\Theta}^{\pm} \\ K_{\phi}^{\pm} \end{matrix}\right\}_{SB} \sim \left\{\begin{matrix} 1 \\ 1 \end{matrix}\right\} \tag{4.42a}$$

and

$$|d_{\pm}|_{SB} \sim \omega_{\pm} \tag{4.42b}$$

Further, in the vicinity of the reflection boundary ($\Theta = \pm\pi$), Eq. 4.40 is approximately

$$\left.\begin{matrix} D_h^{\pm} \\ D_s^{\pm} \end{matrix}\right\}_{RB} \sim \frac{\pm\, e^{-j\frac{\pi}{4}}}{2\sqrt{2\pi k}}\; \frac{F(|d_{\pm}|\, e^{j\frac{\pi}{4}})}{\cos\frac{\Theta}{2}} \left\{\begin{matrix} 1 \\ -1 \end{matrix}\right\} \tag{4.43}$$

since

$$\left.\begin{matrix} K_{\Theta}^{\pm} \\ K_{\phi}^{\pm} \end{matrix}\right\} \frac{1}{\sin\frac{\alpha \mp \Theta}{2}} \Bigg|_{RB} \sim \left\{\begin{matrix} 1 \\ -1 \end{matrix}\right\} \frac{1}{\cos\frac{\Theta}{2}} \tag{4.43a}$$

in the neighborhood of the reflection boundary.

Eqs. 4.42 and 4.43 become equal to half the stationary point contribution at the shadow and reflection boundaries respectively (Eq. G-6). This is because of the fact that, at these boundaries, $\Psi(\alpha,\phi_{\pm})$ (Eq. E-18) is stationary and $d_{\pm}$ goes to zero. Eq. 4.43 still predicts infinite fields at the reflection boundary because of vanishing $\Psi_{\theta\theta}(\alpha,\phi_{\pm})$ at $\Theta = \pm\pi$ (Eqs. E-21 and G-6). In fact, the actual analysis is not valid at this boundary, firsly, because the asymptotic expansion of Bessel functions (Eq. 4.18) are valid only away from the caustics and secondly, as $\Theta \to \pm\pi$ it becomes impossible to identify a large parameter in

the phase function (Eq. E-1) to be able to approximate Eq. 4.10 asymptotically. Bearing in mind that in the neighborhood of shadow boundary Eq. 4.43 is negligibly small compared to Eq. 4.42 and vice versa at the reflection boundary, diffraction coefficients obtained by the summation of Eqs. 4.42 and 4.43

$$D_{h_s}^{+} = \frac{-j\frac{\pi}{4}}{2\sqrt{2\pi k}} \left\{ \frac{F(\omega_+ e^{j\frac{\pi}{4}})}{\sin\frac{\alpha-\theta}{2}} \pm \frac{F(|d_+| e^{j\frac{\pi}{4}})}{\cos\frac{\theta}{2}} \right\} \tag{4.44a}$$

$$D_{h_s}^{-} = \frac{-e^{-j\frac{\pi}{4}}}{2\sqrt{2\pi k}} \left\{ \frac{F(\omega_- e^{j\frac{\pi}{4}})}{\sin\frac{\alpha+\theta}{2}} \pm \frac{F(|d_-| e^{j\frac{\pi}{4}})}{\cos\frac{\theta}{2}} \right\} \tag{4.44b}$$

are valid only in the vicinity of these boundaries.

Comparison of Eqs. 4.41 and 4.44 shows that exept for ε_o and the transition function associated with the reflection boundary, they are the same. Argument of the transition function, in Eq. 4.44. associated with the reflection boundary, vanishes as this boundary is approached (Eq. G-4) while that of GTD tends to infinity (Eq. 3.10). Although this discrepancy does not bring much difference in practice since both methods fail at this boundary, it permits us to conclude that the method followed by GTD to calculate the arguments of the transition functions is not precise enough. GTD can be improved by calculating the argument of transition functions from the first and second derivatives of the phase function (Eq. G-4), which is easy to find from the system geometry.

As far as ε_o is concerned, it is due to the calculation of GTD diffraction coefficient at Q_-; GTD assumes that when the observation point crosses the reflector (see Section 3.2.2 and Fig. 3.4) $D_{h,s}^{-}$ changes sign and in the region where straight line between Q_- and P (the observation point) passes through the reflector ($\frac{\pi-\alpha}{2} < \theta < \frac{\pi}{2}$) diffraction from Q_- does not contribute to the scattered field. Existence of the stationary point whose contribution (geometrical optics term) is cancelled by the direct feed radiation in the shadow region ($\theta < \alpha$) contradicts this assumption of GTD. In order to find $D_{h,s}^{-}$ correctly, a positif direction should be defined (Fig. 4-1) and γ_i^{-} (γ_d^{-}) should be calculated by choosing the smallest angle between the reference plane and

the incident (diffracted) ray by taking into account its sign as well. From Fig. 4-1, we easily find

$$\gamma_i^- = \frac{\pi-\alpha}{2}$$

$$\gamma_d^- = \begin{cases} -\left(\frac{\pi-\alpha}{2} - \theta\right) & \theta < \frac{\pi-\alpha}{2} \\ \theta - \frac{\pi-\alpha}{2} & \theta > \frac{\pi-\alpha}{2} \end{cases} = \theta - \frac{\pi-\alpha}{2} \qquad (4.45)$$

which renders ε_o identically equal to unity for all θ values.
It is important to note that ε_o as defined by Eq. 3.18 makes the GTD solution discontinuous and yields erroneous results in the region $\theta < \frac{\pi-\alpha}{2}$ where it is equal to -1. The reported differences between GTD solution and experimental and physical optics results in the shadow region ($\theta < \alpha$) ([7], [8] and [11]) may be attributed to this discrepancy.
All these considerations simply imply that GTD, even with its corrected diffraction coefficients (Eq. 4.44), can approximate the diffracted rays only in the vicinity of reflection and shadow boundaries. GTD diffraction coefficients (Eq. 4.41) are nothing but approximations to PO diffraction coefficients (Eq. 4.40).

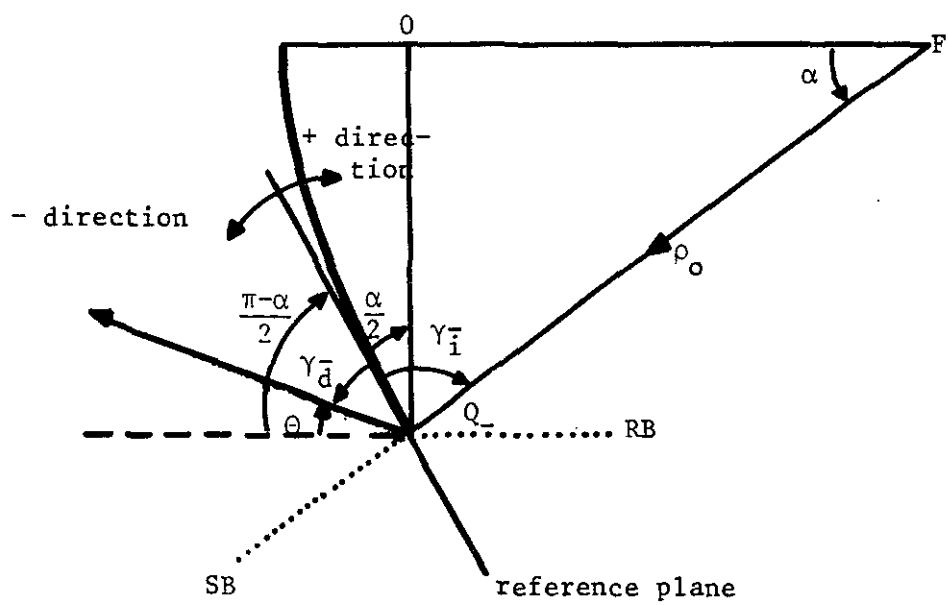

Fig. 4.1. Geometry of incident and diffracted rays for calculating γ_i^- and γ_d^- correctly.

4.5. Analysis at forward and rear directions

In the forward and rear axial directions, because of small values of $\sin\Theta$, Bessel functions in Eq. 4.17 vary slowly. For this reason, in these directions, this integral equation may be evaluated asymptotically without resorting to the asymptotic expansion of Bessel functions.
For the sake of clarity, Eq. 4.17 will be rewritten as

$$\left.\begin{matrix} E_\Theta \\ E_\Phi \end{matrix}\right\} = \int_0^\alpha \left\{\begin{matrix} g_\Theta(\theta) \\ g_\Phi(\theta) \end{matrix}\right\} e^{-jq(\theta)}\, d\theta \tag{4.46}$$

where

$$\left.\begin{matrix} g_\Theta(\theta) \\ g_\Phi(\theta) \end{matrix}\right\} = \left\{\begin{matrix} \sin\Phi \\ \cos\Phi \end{matrix}\right\} k\rho\sin\theta\sqrt{G_f(\theta)}\left[-j\left\{\begin{matrix} \cos\Theta \\ 1 \end{matrix}\right\} J_0(\beta)\,\frac{u_\theta+1}{2}\right.$$

$$\left. + j\left\{\begin{matrix} \cos\Theta \\ -1 \end{matrix}\right\} J_2(\beta)\,\frac{u_\theta-1}{2} + \left\{\begin{matrix} \sin\Theta \\ 0 \end{matrix}\right\} u_\theta \tan\frac{\theta}{2}\, J_1(\beta)\right] \tag{4.47}$$

$$q(\theta) = k\rho(1-\cos\theta\cos\Theta) = 2kf - k\rho\cos\theta(1+\cos\Theta) \tag{4.48}$$

and

$$\beta = k\rho\sin\theta\sin\Theta \tag{4.16}$$

From Eq. 4.48, it is easy to calculate

$$q_\theta(\theta) = k\rho\tan\frac{\theta}{2}(1+\cos\Theta) \tag{4.49}$$

$$q_{\theta\theta}(\theta) = k\rho\sec^2\frac{\theta}{2}\left(1-\frac{1}{2}\cos\theta\right)(1+\cos\Theta) \tag{4.50}$$

4.5.1. Forward radiation

Eq. 4.48 clearly shows that in the neighborhood of forward direction ($\Theta \to \pm\pi$), it is impossible to identify a large parameter in $q(\theta)$ rendering an

asymptotic evaluation of Eq. 4.40 possible. We can again observe that $q(\theta)$ does not considerably change in that region thus somewhat facilitating the analysis. From Eq. 4.48, for the values of Θ such that

$$\max\left\{ k\rho\cos\theta(1+\cos\Theta)\right\} = kf(1+\cos\Theta) < \Psi_F \tag{4.51}$$

where Ψ_F approximately satisfies the relations

$$\cos\Psi_F \approx 1 \tag{4.52a}$$

$$\sin\Psi_F \approx 0 \tag{4.52b}$$

the phase term in Eq. 4.46 can be taken out of the integral sign. Eq. 4.51 is evidently satisfied over the main beam and a few sidelobes around it. With this approximation, Eq. 4.46 reduces to

$$\left.\begin{matrix} E_\Theta \\ E_\Phi \end{matrix}\right\} \cong e^{-j2kf} \int_0^\alpha \left\{ \begin{matrix} g_\Theta(\theta) \\ g_\Phi(\theta) \end{matrix} \right\} d\theta \tag{4.53}$$

For Huygens source feeding ($u_\theta = 1$), Eq. 4.53 may approximately be written as

$$\left.\begin{matrix} E_\Theta \\ E_\Phi \end{matrix}\right\}^{HUY} \cong \left\{ \begin{matrix} \cos\Theta\sin\Phi \\ \cos\Phi \end{matrix} \right\} e^{-j\left(2kf+\frac{\pi}{2}\right)} \int_0^\alpha k\rho\sin\theta\, J_0(k\rho\sin\theta\sin\Theta) \frac{\sqrt{G_f(\theta)}}{k\rho} k\rho d\theta \tag{4.54}$$

which is proportional to the Hankel transform of the aperture distribution given by

$$\mathcal{F}(\theta) = \frac{\sqrt{G_f(\theta)}}{k\rho} \tag{4.55}$$

The method of calculating the scattered field by Eq. 4.54 is known as the scalar aperture method [15] and its validity limit is determined by Eqs. 4.51 and 4.52.

In the forward direction ($\Theta = \pm\pi$), Eq. 4.46 is equal to

$$\left.\begin{matrix} E_\theta \\ E_\Phi \end{matrix}\right]_F = \left\{\begin{matrix} -\sin\Phi \\ \cos\Phi \end{matrix}\right\} e^{-j(2kf+\frac{\pi}{2})} \int_0^\alpha k\rho\sin\theta \sqrt{G_f(\theta)}\ \frac{u_\theta+1}{2}\ d\theta \qquad (4.56)$$

For dipole feeding ($u_\theta = \cos\theta$), amplitude of the electric field vector is from Eq. 4.56

$$E_F^{DIP} = \frac{1}{2} ka\cot\frac{\alpha}{2} \int_0^\alpha \sin\theta \sqrt{G_f(\theta)}\ d\theta \qquad (4.57)$$

where by virtue of Eq. 4.2

$$f = \frac{a}{2}\cot\frac{\alpha}{2} = \frac{D}{4}\cot\frac{\alpha}{2} \qquad (4.58)$$

Eq. 4.57 reduces to;
For uniform aperture distribution (Eq. 2.8)

$$E_{F,u}^{DIP} = 2ka\ \cot^2\frac{\alpha}{2}\ \left|\ln\cos\frac{\alpha}{2}\right| \qquad (4.59)$$

and for the feed patterns given by Eq. 2.7

$$E_{F,n}^{DIP} = \frac{\sqrt{2(n+1)}}{n+2} ka\cot\frac{\alpha}{2}\left[1-(\cos\alpha)^{1+\frac{n}{2}}\right] \qquad n=1,2,3\ldots \qquad (4.60)$$

For Huygens source feeding ($u_\theta = 1$), Eq. 4.56 is equal to

$$E_F^{HUY} = ka\cot\frac{\alpha}{2} \int_0^\alpha \tan\frac{\theta}{2} \sqrt{G_f(\theta)}\ d\theta \qquad (4.61)$$

from which we can easily find

$$E_{F,u}^{HUY} = ka \qquad (4.62)$$

$$E_{F,2n-1}^{HUY} = \sqrt{2(n+1)}\; 2ka\cot\frac{\alpha}{2}\; M_{2n-1} \qquad n=1,2,3... \qquad (4.63)$$

where

$$M_{2n-1} = \frac{1-(\cos\alpha)^{n-\frac{1}{2}}}{2n-1} - M_{2n-3} \qquad (4.63a)$$

with

$$M_{-1} = \frac{\pi}{4} - \tan^{-1}\sqrt{\cos\alpha} \qquad (4.63b)$$

For even values of n

$$E_{F,n}^{HUY} = 2\sqrt{2(n+1)}\; ka\cot\frac{\alpha}{2}\left|\sin^{n}\frac{\alpha}{2} + \ln\cos\frac{\alpha}{2}\right| \qquad n=2 \text{ and } 4 \qquad (4.64)$$

$$E_{F,6}^{HUY} = \sqrt{14}\; ka\cot\frac{\alpha}{2}\left|2\ln\cos\frac{\alpha}{2} + \frac{(1-\cos\alpha)^3}{3} + \frac{1}{2}\sin^2\alpha\right| \qquad (4.65)$$

$$E_{F,8}^{HUY} = \sqrt{18}\; ka\cot\frac{\alpha}{2}\left|\frac{1-\cos^4\alpha}{2} - 2\ln\cos\frac{\alpha}{2} - \frac{(1-\cos\alpha)^3}{3} - \frac{\sin^2\alpha}{2}\right| \qquad (4.66)$$

It is important to note that Eqs. 4.57 and 4.61 are equal to the square root of the antenna gain for dipole and Huygens source feeds respectively.
Eq. 4.59 to 4.65 are drawn in Fig. 4.2 versus α after being normalised with respect to ka whose square is equal to the gain of a uniformly illuminated paraboloid having a Huygens source feed (Eq. 4.62).
Fig. 4.2 clearly shows that the gain for Huygens source feeding is higher than that for dipole feeding having the same feed pattern. This is due to the fact that dipole feeding yields more tapered aperture distributions in the E-plane because of u_θ factor in its polarisation vector (Eqs. 2.5 and 2.6).

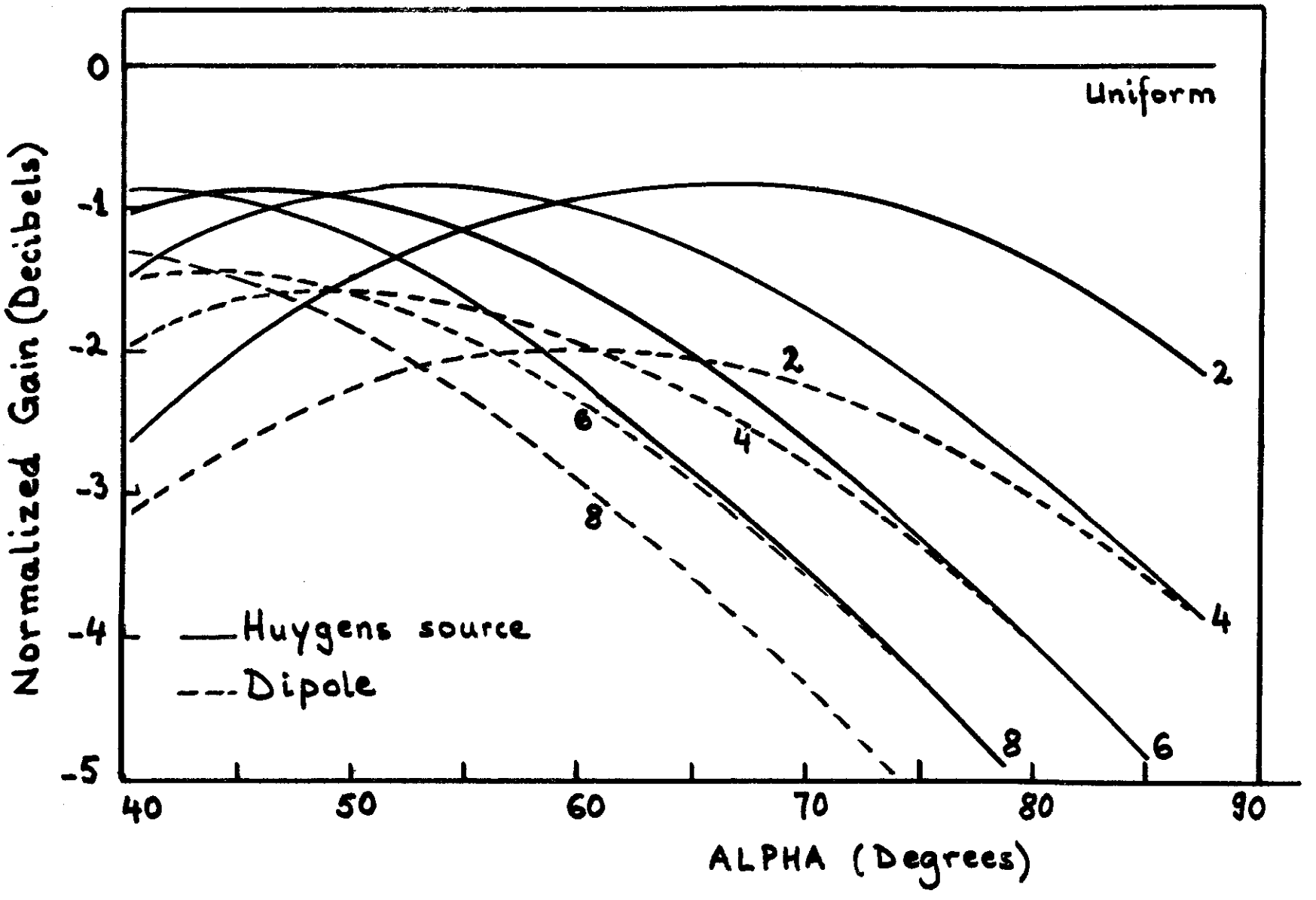

Fig. 4.2. Normalized gain of a paraboloid for dipole and Huygens source feeds.

4.5.2. Rear radiation

Eq. 4.49 shows that in the neighborhood of the rear caustic, $q(\theta)$ has a stationary point at $\theta = 0$. Since the integral kernel (Eq. 4.47) vanishes at this point, the only contribution to the asymptotic expansion of Eq. 4.46 comes from the end point.
From Eq. 4.46 and Eq. C-5, one easily gets

$$\left.\begin{matrix} E^t_\theta \\ E^t_\phi \end{matrix}\right\} = \left\{\begin{matrix} \sin\phi \\ \cos\phi \end{matrix}\right\} \frac{1+\cos\alpha}{1+\cos\theta} \sqrt{G_f(\alpha)}\; e^{-jq(\alpha)} \cdot$$

$$\left[J_0(v) \frac{1+u_\alpha}{2} \left\{\begin{matrix} \cos\theta \\ 1 \end{matrix}\right\} + J_2(v) \frac{u_\alpha - 1}{2} \left\{\begin{matrix} -\cos\theta \\ 1 \end{matrix}\right\} + j u_\alpha \tan\frac{\alpha}{2} J_1(v) \left\{\begin{matrix} \sin\theta \\ 0 \end{matrix}\right\} \right] \tag{4.67}$$

where

$$v = ka \sin\theta \tag{4.67a}$$

As already been mentioned, the above formula is valid only for small values of β (defined by Eq. 4.16) which is evidently satisfied in the neighborhood of the caustic regions. Because of its simplicity, it is a useful formula for calculating the rear radiation. Fig. 4.3 shows the comparison of Eqs. 4.34, 4.67 and the GTD solution (Eq. 3.21) for Huygens source feeding. The two asymptotic physical optics solutions smoothly join each other as the rear caustic direction is approached, as expected. For this reason, they are complementary and enough to describe the rear radiation. Equivalent edge currents method ([12] to [14]) currently used for this purpose is cumbersome and incorrect since it is derived from GTD. GTD prediction for rear radiation does not agree with physical optics solutions. As already explained in Ch. 3 and section 4.4. this is because of the fact that GTD can predict the scattered field correctly only in the near vicinity of reflection and shadow boundaries. Amplitude of the back radiated field is found by inserting $\theta = 0$ in Eq. 4.67

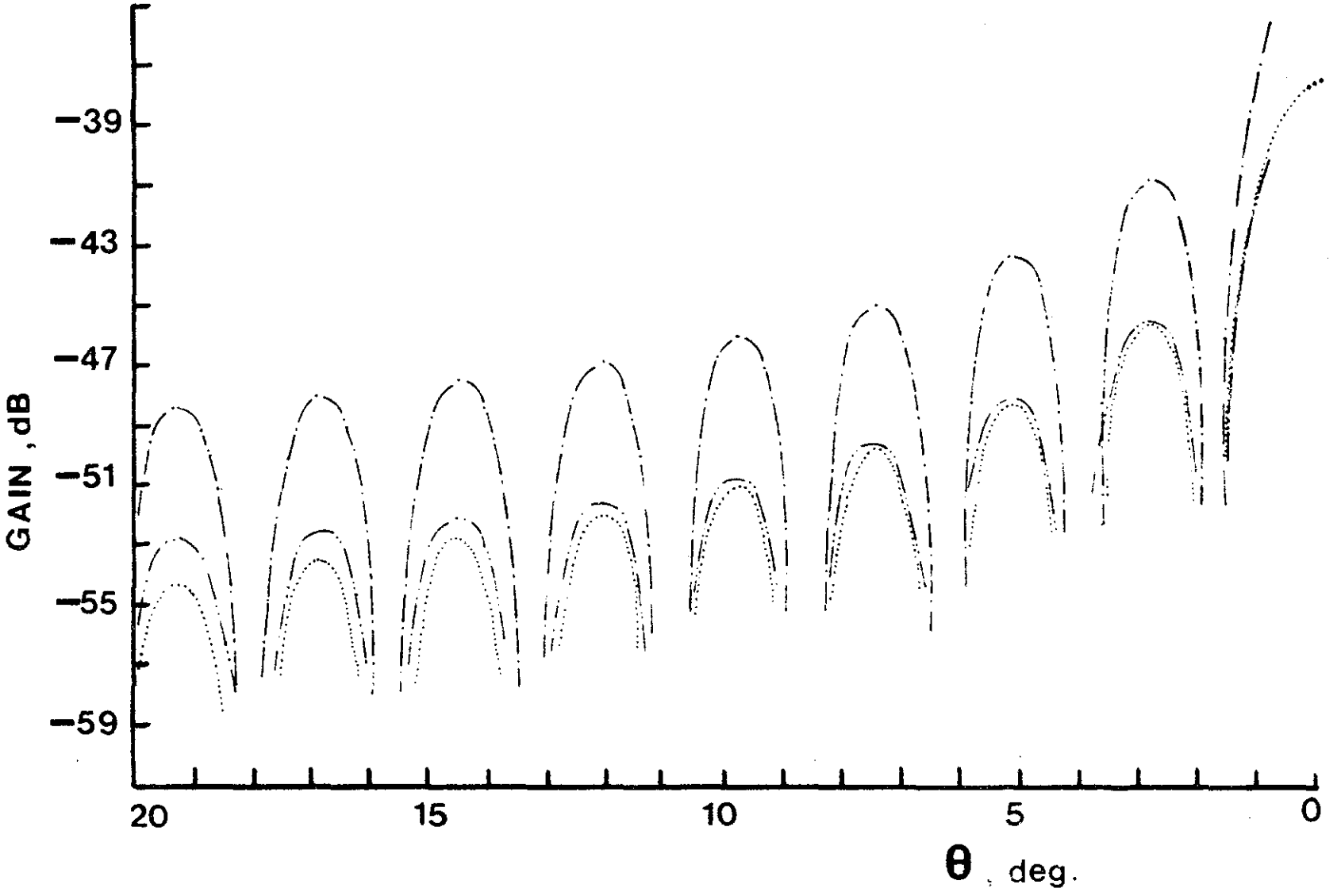

Fig. 4.3. E-plane rear radiated field of a paraboloid with Huygens source feed at focus.
$D = 25\lambda$, $\alpha = 60^{o}$ and $n = 2$.
-.- GTD, Eq. 3.21
-..- APO, Eq. 4.34
..... Eq. 4.67

$$E_B = \sqrt{G_f(\alpha)} \quad \frac{1+\cos\alpha}{2} \quad \frac{1+u_\alpha}{2} \tag{4.68}$$

It is interesting to note that the back radiated electromagnetic field for dipole feeding is $\frac{1+\cos\alpha}{2}$ times smaller than that for Huygens source feeding which is, of course, due to its lower edge illumination in E-plane.
Inserting Eq. 2.8 into Eq. 4.68, we obtain the back radiation of a uniformly illuminated paraboloid as

$$E_{B,UN}^{HUY} = \cot\frac{\alpha}{2} \tag{4.69}$$

4.5.3. Front to back ratio

Back radiation from paraboloid bears particular importance in calculating the antenna noise and the interference between different communication systems. In this section relative level of the back radiated field with respect to the front radiation will be calculated and its relation to other antenna parameters will be studied.
Front to back ratio, which is defined to be

$$F/B = 20\log\left\{\frac{\sqrt{\eta_a}\,|E_F|}{|E_B|}\right\} = G - 20\log|E_B| \quad (dB), \tag{4.70}$$

is a measure of the relative level of back radiation with respect to the front radiation. η_a is the antenna efficiency and the antenna gain is defined by

$$G = 20\log\left\{\sqrt{\eta_a}\,|E_F|\right\} \quad (dB) \tag{4.71}$$

where E_F is given by Eqs. 4.59 to 4.66 and E_B by Eq. 4.68.
As studied in the previous chapter the most significant contribution to the back radiated field comes from the paraboloid edge illumination. For this reason, there is a close relationship between the feed taper at the paraboloid edge and the back radiated field. Feed taper is defined to be the ratio of average of E- and H-plane edge illuminations to peak feed radiation, i.e.

$$T_F = \frac{\sqrt{G_f(\alpha)}\ \frac{1+u_\alpha}{2}}{\sqrt{G_f(0)}} = \cos^{\frac{n}{2}}\alpha \quad \frac{1+u_\alpha}{2} \tag{4.72a}$$

and in decibels

$$T_F = 10\ n\ \log|\cos\alpha| + 20 \log\left(\frac{1+u_\alpha}{2}\right) \quad (dB) \tag{4.72b}$$

Taper of the aperture distribution is similarly

$$T_{AD} = \frac{\mathcal{F}(\alpha)}{\mathcal{F}(0)} = \sqrt{\frac{G_f(\alpha)}{G_f(0)}}\ \frac{1+\cos\alpha}{2}\ \frac{1+u_\alpha}{2} \tag{4.73a}$$

where $\mathcal{F}(\theta)$ is defined by Eq. 4.55. In decibels,

$$T_{AD} = T_F + 40 \log|\cos\tfrac{\alpha}{2}| \quad (dB) \tag{4.73b}$$

T_F and T_{AD} are shown in Fig. 4.4 versus α for Huygens source polarised feed. It is interesting to observe (Eqs. 4.68 and 4.73a) that the back radiated field is equal to

$$E_B = \sqrt{G_f(0)}\ T_{AD}$$

where $G_f(o)$ is proportional to the feed gain. Thus

$$E_B = G_F + T_{AD} = G_F + T_F + 40 \log|\cos\tfrac{\alpha}{2}| \quad (dB) \tag{4.74}$$

where

$$G_F = 10 \log G_f(0) \tag{4.75}$$

Back radiated field from Eq. 4.74 is drawn in Fig. 4.5 versus feed taper. From Eqs. 4.70 and 4.74, F/B ratio may be rewritten as

$$F/B = G - G_F - T_F - 40 \log|\cos\tfrac{\alpha}{2}| \quad (dB) \tag{4.76}$$

Defining

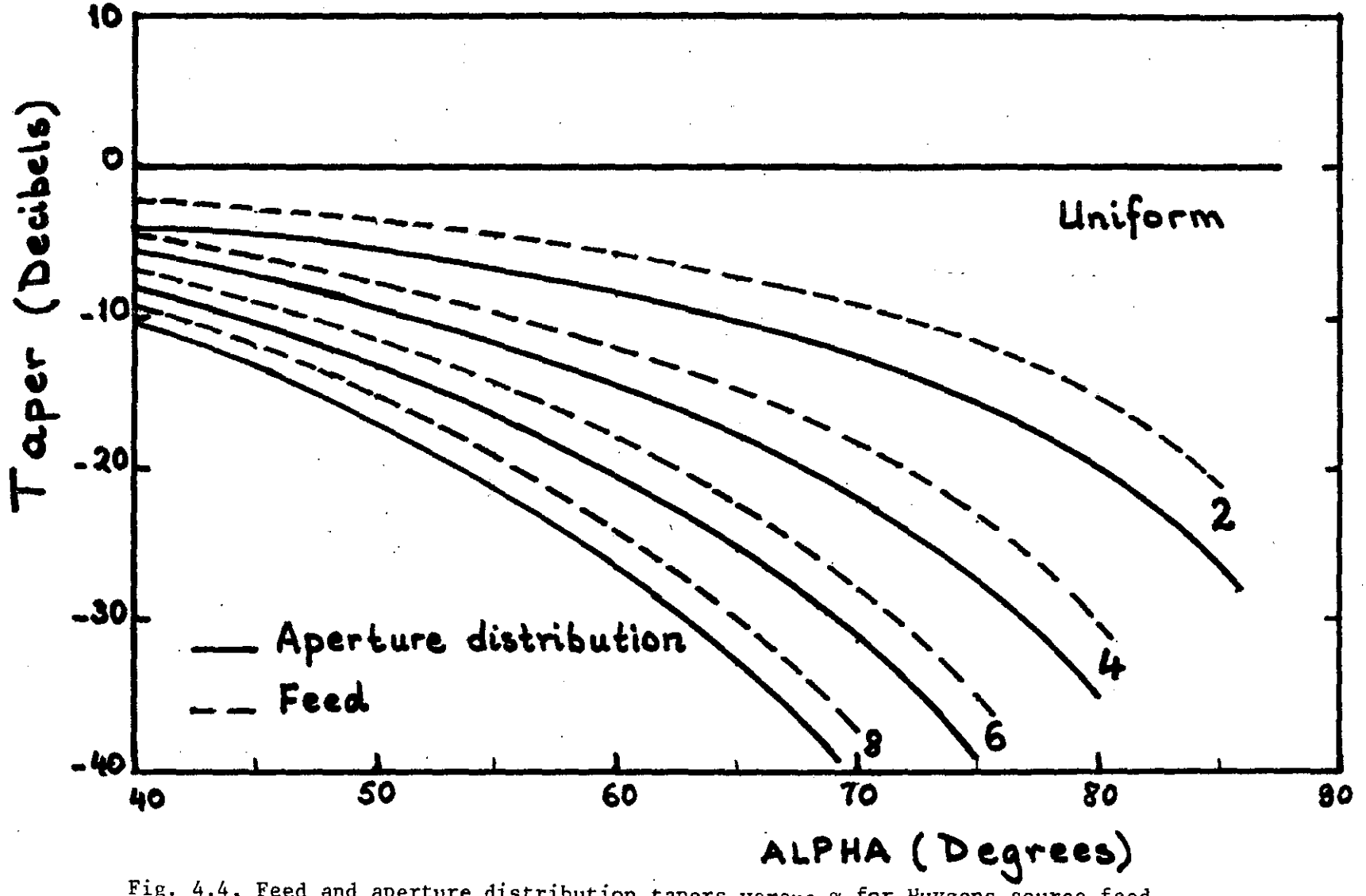

Fig. 4.4. Feed and aperture distribution tapers versus α for Huygens source feed.

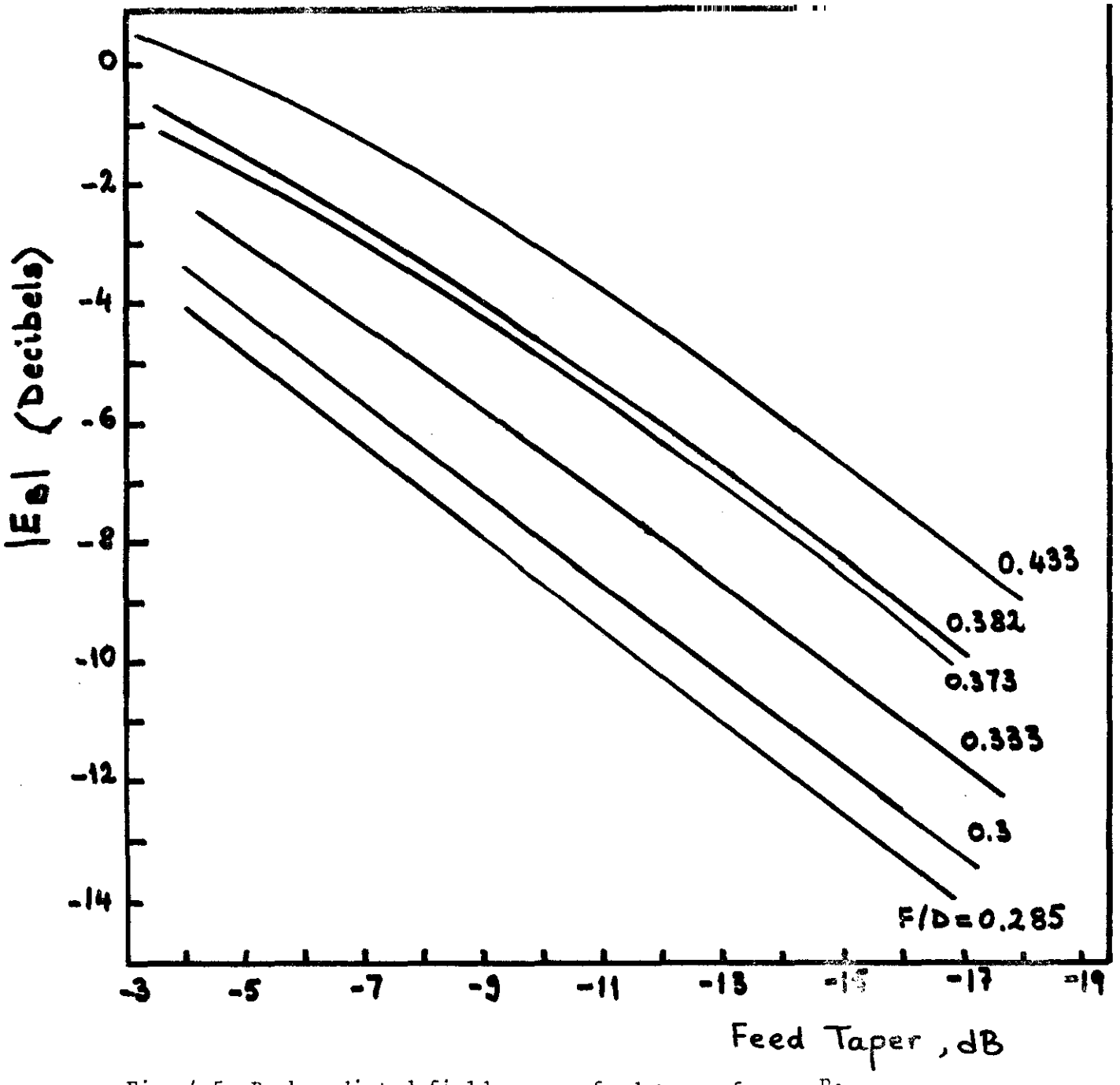

Fig. 4.5. Back radiated field versus feed taper for $\cos^n\theta$ patterns.

$$K = -20 \log \left| \cos \frac{\alpha}{2} \right| \qquad (dB) \tag{4.77}$$

which is identical to ([24], Eq. 21), we observe that back radiation given by Eq. 4.74 is K dB lower than that given by Knop ([24], Eq. 8). More explicitely, to find E_B and F/B ratio given by Knop ([24], Eqs. 8 and 20), K should be added to and subrected from Eqs. 4.74 and 4.76 respectively. It is interesting to write F/B ratio of a uniformly illuminated paraboloid; from Eqs. 4.62, 4.69 and 4.70

$$F/B\Big|_{UN}^{HUY} = 20 \log \left| \sqrt{\eta_a}\, ka \tan \frac{\alpha}{2} \right| \qquad (dB) \tag{4.78}$$

which differs from the result of Knop ([24], Eq. 12) by the same factor K given by Eq. 4.77.

The above-cited discrepancies between our results and those of Knop may be attributed to the errors in equivalent edge current method utilised by Knop to predict the rear radiated fields.

Front/Back ratio of a paraboloid is shown versus feed taper, n and α respectively in Figs. 4.6 to 4.8 after being normalised with respect to $(ka)^2$, gain of a 100% efficient uniformly illuminated paraboloid.

From the above figures, it is apparent that with increasing α and n, which increase the edge taper (Eq. 4.72), F/B ratio also increases. On the other hand, F/B ratio for dipole feeding is higher than that for Huygens source feeding because of its more tapered edge illumination. Although the antenna gain for dipole polarisation is lower, this is compensated by its lower edge illumination yielding lower sidelobes and back radiation.

It is interesting to compare our results for F/B ratio with those of Knop ([24], Table I) who utilised equivalent edge currents method to calculate the back radiation and the measured antenna gain for front radiation. The results are shown in Table 4.2. Normalised F/B ratio is readily observable from Fig. 4.6 for different feed tapers and F/D ratios and ka is given in decibels. The sum of these two yield the theoretical F/B ratio, (for a 100% efficient paraboloid). Using the measured gain which Knop gives and the back radiation from Fig. 4.5 a more realistic estimate of the F/B ratio is given in the last colomn.

Comparison of our results with those of Knop shows that F/B ratios given by Knop

at 1.905 GHz and some others for other frequencies are even higher that those of a 100% efficient paraboloid. This implies very large error limits in his F/B ratio measurements. Further, because of already observed errors in rear radiated field and F/B, theoretical results given by Knop [24] are not reliable. On the other hand, gain and F/B ratio of antennas having the same F/D should decrease 2.42 dB, 5.17 dB, 3.88 dB and 6.33 dB when the operating frequency is changing from 14.8 GHz to 11.2 GHz, 11.2 GHz to 6.175 GHz, 6.175 GHz to 3.95 GHz and 3.95 GHz to 1.905 GHz respectively.
This is because of the linear dependence of gain and F/B ratio to ka (Eq. 4.76). A direct observation from Table 4.2 shows that Knop's results are far from satisfying this condition either.

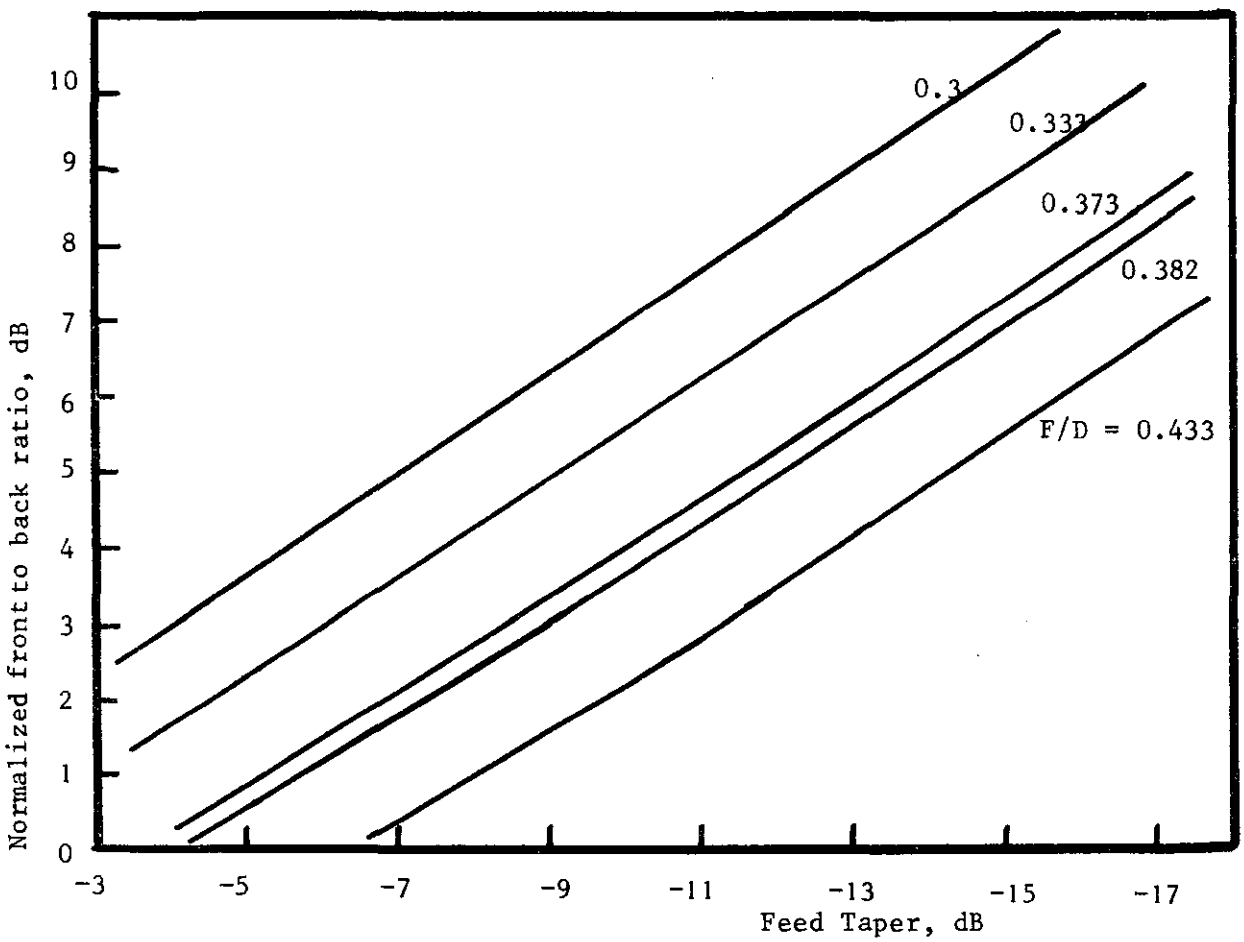

Fig. 4.6 Normalized front to back ratio versus feed taper for a Huygens source feed at focus.

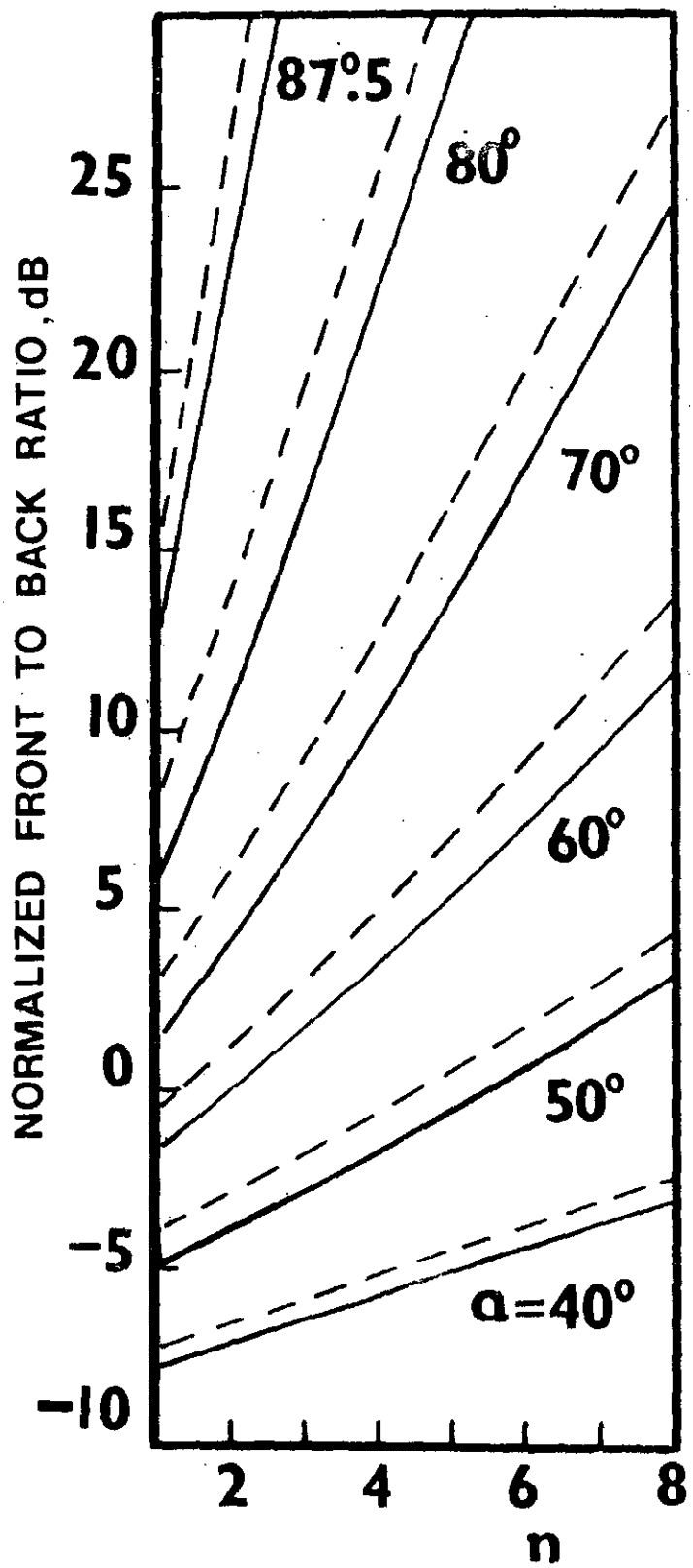

Fig. 4.7 Normalized front to back ratio of a focus-fed paraboloid versus n with α as a parameter
--- dipole feed
____ Huygens source feed.

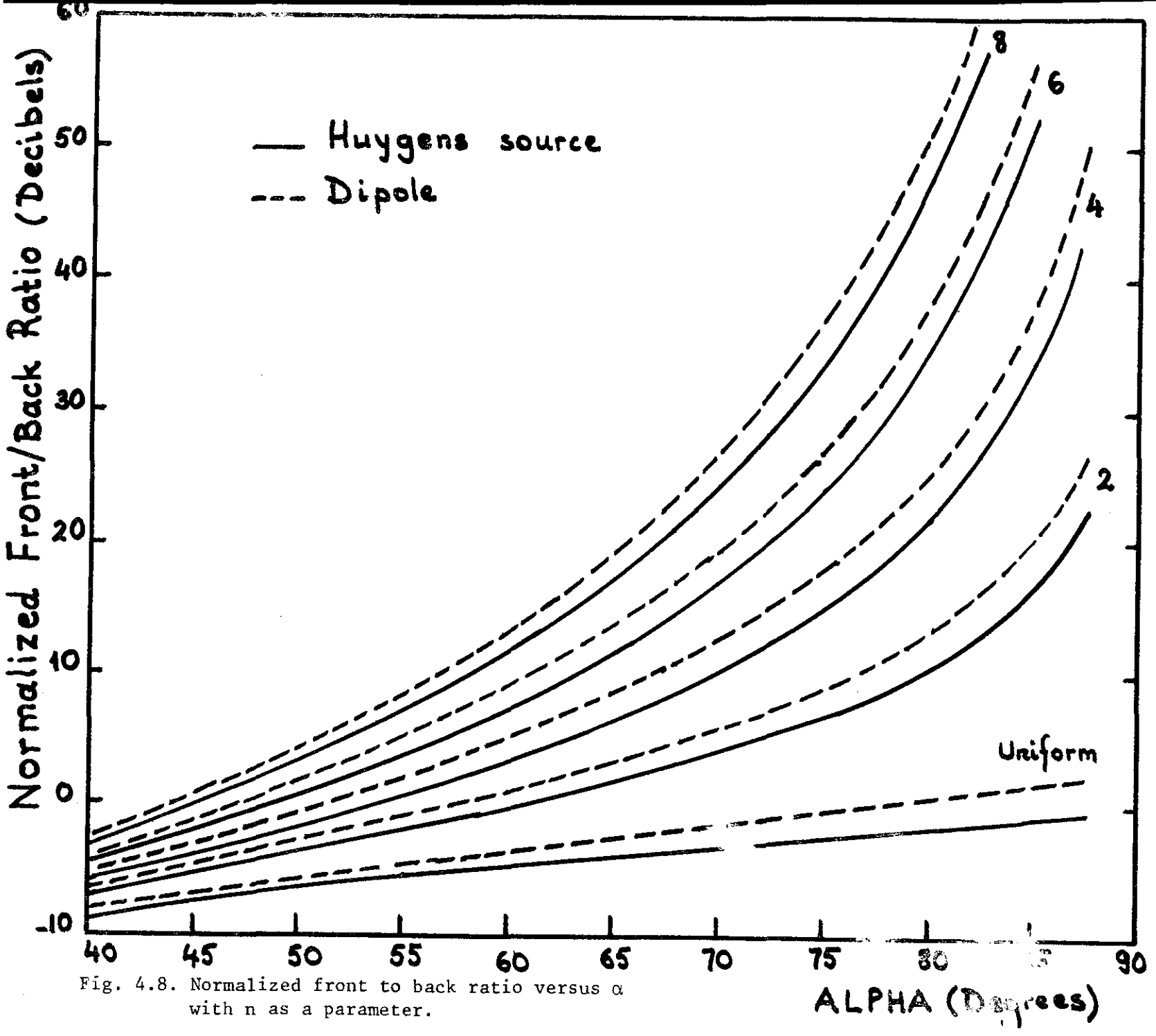

Fig. 4.8. Normalized front to back ratio versus α with n as a parameter.

Knop ([24], Table 1)							Safak				
D (ft)	F/D	T_F (dB)	G (dB)	Freq. (GHz)	F/B (meas)	F/B (calcul.)	Normal. F/B	ka (dB)	Theor. F/B (dB)	$\|E_B\|$ (dB)	Exper. F/B (dB)
4	0.375	-5	18,4	0.925	21	21.0	0.85	21.4	22.25	-1.7	20.1
6	0.382		22.0		24	24.6	0.55	24.97	25.53	-0.5	22.5
8	0.373		24.4		27	27.0	1	27.5	28.5	-1.8	26.2
10	0.300		26.4		29	29.7	3.7	29.4	33.1	-4.2	30.6
12	0.333		28.0		30	30.9	2.3	30.97	33.27	-3.1	31.1
15	0.333		29.9		32	32.8	2.3	32.9	35.2	-3.1	33.0
6	0.382	-10	28.7	1.905	36	37.0	3.65	31.24	34.89	-4.6	33.3
8	0.373		31.2		39	39.6	4	33.74	37.74	-4.9	36.1
10	0.300		33.2		44	42.3	7	35.7	42.7	-8.0	41.2
12	0.333		34.7		45	43.4	5.6	37.2	42.8	-6.5	41.2
15	0.333		36.6		47	45.3	5.6	39.2	44.8	-6.5	43.1
6	0.382	-10	35.0	3.95	40	40.0	3.65	37.57	41.22	-4.6	39.6
8	0.373		37.3		41	42.4	4	40.1	44.1	-4.9	42.2
10	0.300		39.3		47	45.1	7	42.0	49.0	-8	47.3
12	0.333		41.0		50	46.4	5.6	43.6	49.2	-6.5	47.5
15	0.333		42.7		52	48.1	5.6	45.53	51.13	-6.5	49.2
6	0.382	-10	38.9	6.175	46	44.5	3.65	41.46	45.11	-4.6	43.5
8	0.373		41.5		48	47.0	4	44.96	48.96	-4.9	46.4
10	0.300		43.3		51	49.6	7	45.9	52.9	-8.0	51.3
12	0.333		45.0		52	50.9	5.6	47.46	53.06	-6.5	51.5
15	0.333		46.4		53	52.3	5.6	49.41	55.01	-6.5	52.9
4	0.375	-10	40.5	11.2	46	46.0	3.85	43.1	46.95	-4.8	45.3
6	0.382		44.0		51	49.5	3.65	46.63	50.28	-4.6	48.6
8	0.373		46.4		52	51.9	4	50.13	54.13	-4.9	51.3
10	0.300		48.3		54	54.5	7	51.1	58.1	-8	56.3
12	0.333		49.8		55	55.6	5.6	52.63	59.23	-6.5	56.3
4	0.375	-10	42.5	14.8	48	49.1	3.85	45.5	49.35	-4.8	47.3
6	0.382		46.1		55	52.7	3.65	49.05	52.7	-4.6	50.7

Table 4.2

Comparison of the obtained front to back ratios with those of Knop.

4.6. Results

In this section calculated GTD and APO radiation patterns are compared in E- and H-planes, effects of feed polarisation and taper on the antenna performance are investigated.

It is important to note that in all the figures to follow, contrary to the definition used until here, θ is measured from the broadside direction. Besides, the radiation patterns are normalised with respect to their broadside gains given by Eqs. 4.59 to 4.66. Normalised back radiation (i.e. -F/B ratio given by Eq. 4.76) is denoted in the following figures so as to test the convergence of asymptotic patterns in the rear direction.

In the preceeding sections, we already observed that GTD can predict the diffracted field correctly only in the neighborhood of reflection and shadow boundaries and yield erroneous results in the shadow region. For this reason a good agreement between two methods in these two regions is expected. The extent to which GTD approaches the results of APO outside these regions may be considered as a measure of validity of this formulation.

Since Eqs. 4.34 and 4.35 are both asymptotic solutions of Eq. 4.1, it is assumed that they yield practically the same diffracted fields. Because of this reason, as APO solution,only Eq. 4.34 is considered. GTD radiation pattern is given by Eq. 3.21.

Before going into details, it should also be mentioned that the calculations are carried out for a paraboloid of 15λ diameter and having a subtended angle of $2\alpha = 120^{\circ}$ ($f/D = 0.433$). It is now a known fact that for paraboloids of diameter larger than $3 - 4\lambda$, asymptotic approximation yield satisfactory results (see Eq. 4.18). Increase in the antenna diameter, although it does not alter the sidelobes' envelopes, increases the number sidelobes of the radiation pattern and reduces the error involved in the asymptotic approximation. For this reason, a $D = 15\lambda$ paraboloid which already bears the characteristics of large antennas gives enough idea about the antenna performance. On the other hand, since the change in subtended angle is directly related to feed taper (Eq. 4.72), the present analysis, where its effect is studied, gives enough insight about the influence of α on radiation patterns.

Eqs. 4.9 and 4.10 show H-plane patterns for Huygens source and dipole feed polarisations respectively. The feed pattern considered is given by Eq. 2.7 with $n = 2$. We observe that the whole radiation pattern for Huygens source feeding is shifted in 1.08 dB below that for dipole feeding. Since the feed

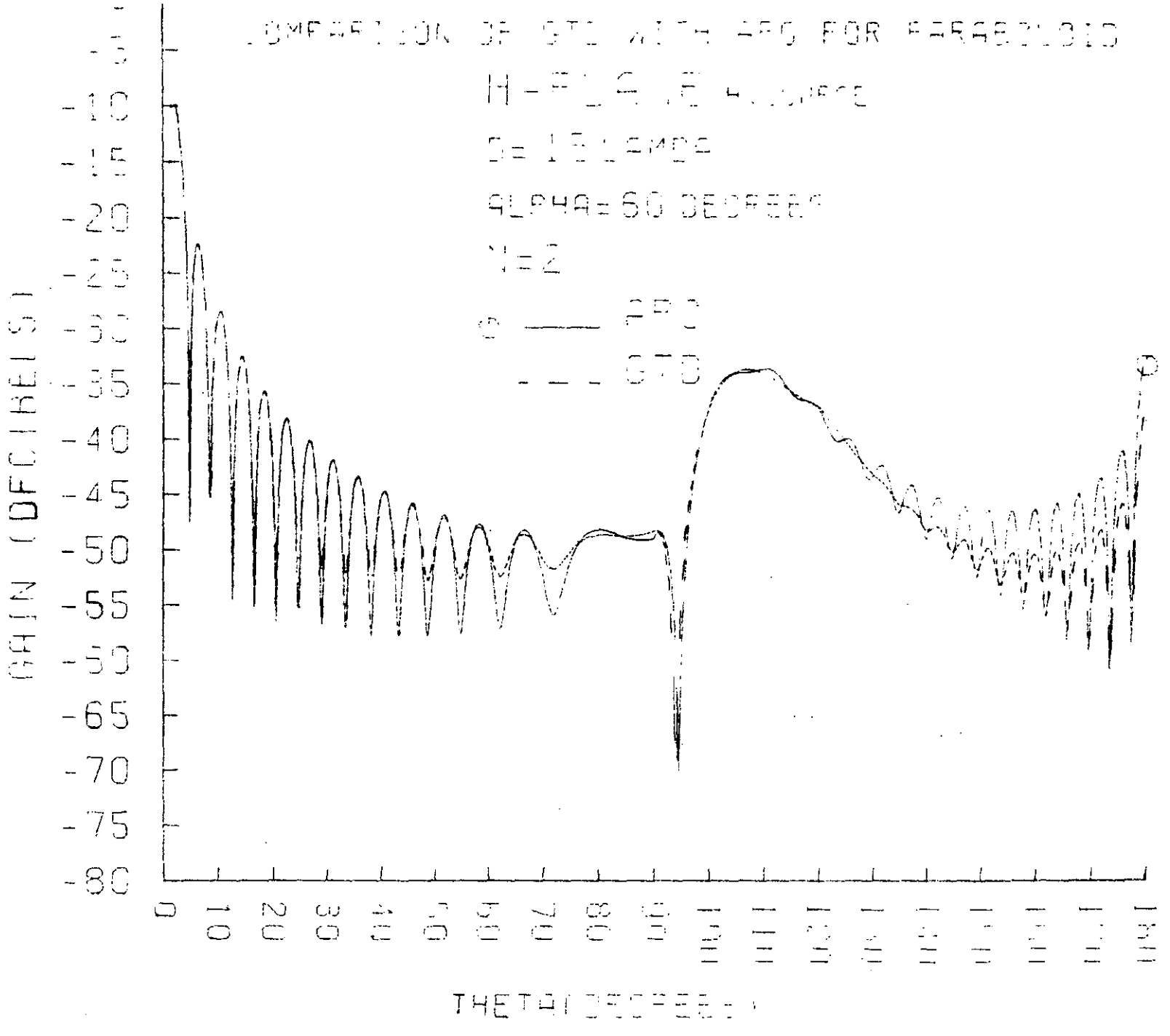

Fig. 4.9 H-plane radiation pattern of a paraboloid with a Huygens source feed at fo

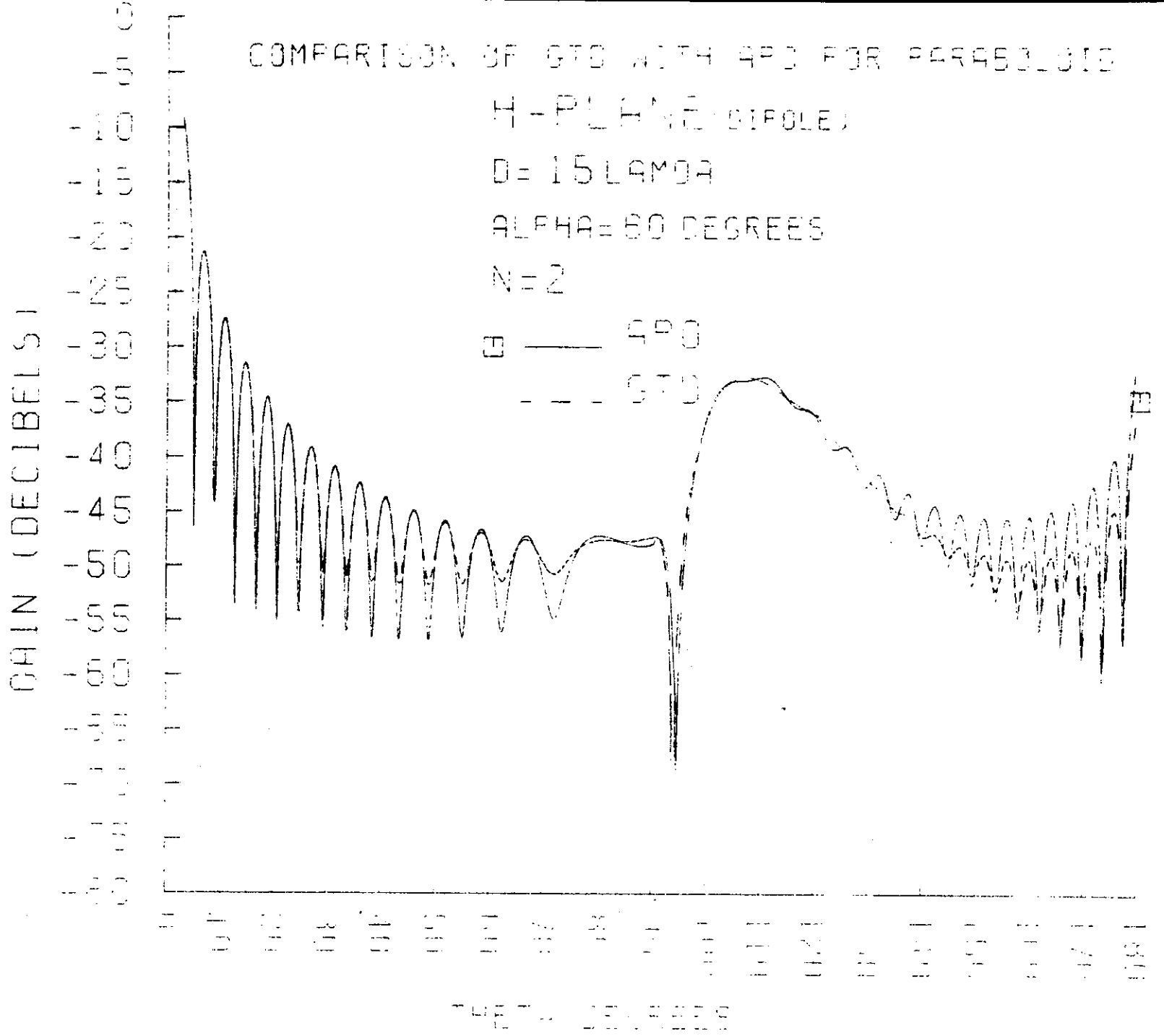

Fig. 4.10 H-plane radiation pattern of a paraboloid with a dipole feed at focus.

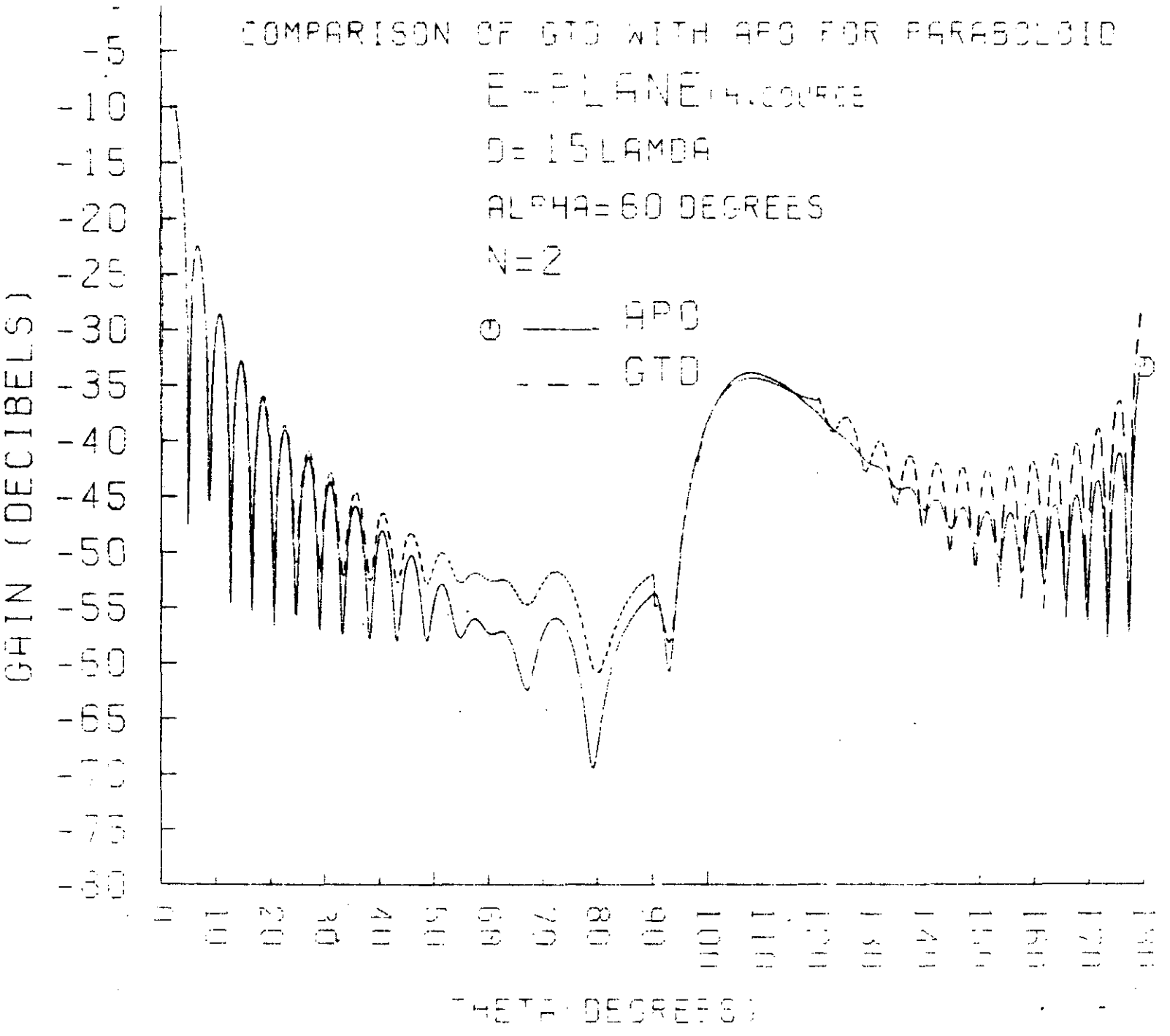

Fig. 4.11 E-plane radiation pattern of a paraboloid with a Huygens source feed at focus.

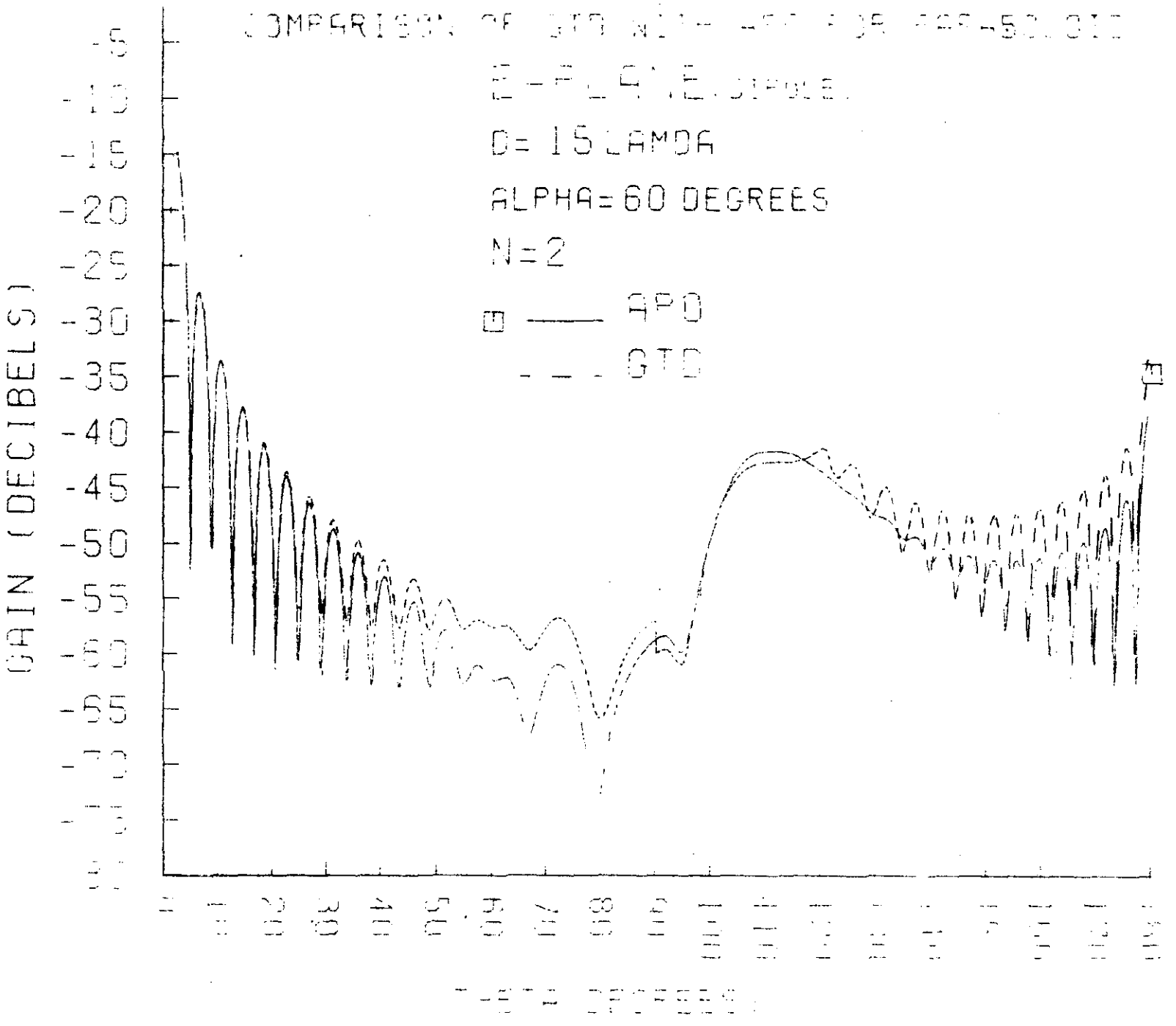

Fig. 4.12 E-plane radiation pattern of a paraboloid with a dipole feed at focus.

tapers at the paraboloid edge are equal for the above cited feeders in this plane, this shift is equal to the difference between the gain for Huygens source feeding (32.56 dB) and that for dipole feeding (31.48 dB).
GTD and APO radiation patterns agree quite closely everywhere except in the shadow region. This discrepancy in the shadow region is expected due to the errors in GTD formulation. The good agreement in the off-shadow region may be attributed to the fact that for the incident electric field vector parallel to the edge, the paraboloid as well as any other reflector locally looks like a straight half plane, for which the GTD formulation is exact [25]. The same argument can not be made for E-plane patterns, on which the reflector surface curvature has a large influence; in the off-shadow region away from the reflection and shadow boundaries, $\hat{z}$-directed currents induced on the paraboloidal surface has a nonnegligible radiation in E-plane but do not radiate in H-plane (Eq. 4.17). This is clearly seen from Figs. 4.11 and 4.12.
E-plane radiation patterns for dipole and Huygens source feeds are compared in Fig. 4.13. The pattern of the former has lower sidelobes because of its lower feed taper in this plane in spite of the higher gain of the latter; in the E-plane, taper of a dipole feed, because of u_α, is 6 dB lower than that for Huygens source feed. Owing to 1.08 dB difference in gain (Table 4.3), the pattern of dipole polarised feed is 4.82 dB shifted downward relative to that of Huygens source feed.
Table 4.3 shows the influence of n on the antenna gain, feed taper and first sidelobe level in E- and H-planes for the afore-mentioned feed polarisations. From Table 4.3 and Fig. 4.2 and 4.4,it is obvious that the sidelobe levels are more sensitive than the antenna gain against n (and the feed taper); for example, increasing n from 2 to 6, decreases the gain by 0.65 dB but accompanies as well a decrease in the first sidelobe level by an amount of about 8 dB. For the sake of completeness, Fig. 4.14 shows the E-plane pattern of a Huygens source fed paraboloid for n = 6.
It is a known fact that paraboloid reflectors with Huygens source feed yielding uniform field distribution on the aperture plane radiate very low cross-polarised fields [26]. Further, uniform field distribution over the antenna aperture results in maximum directivity. From all these considerations, it can easily be concluded that, Huygens source feeds yielding nearly uniform aperture distributions except for a highly tapered edge illumination are ideal for antennas intended to use for dual polarisation purposes.

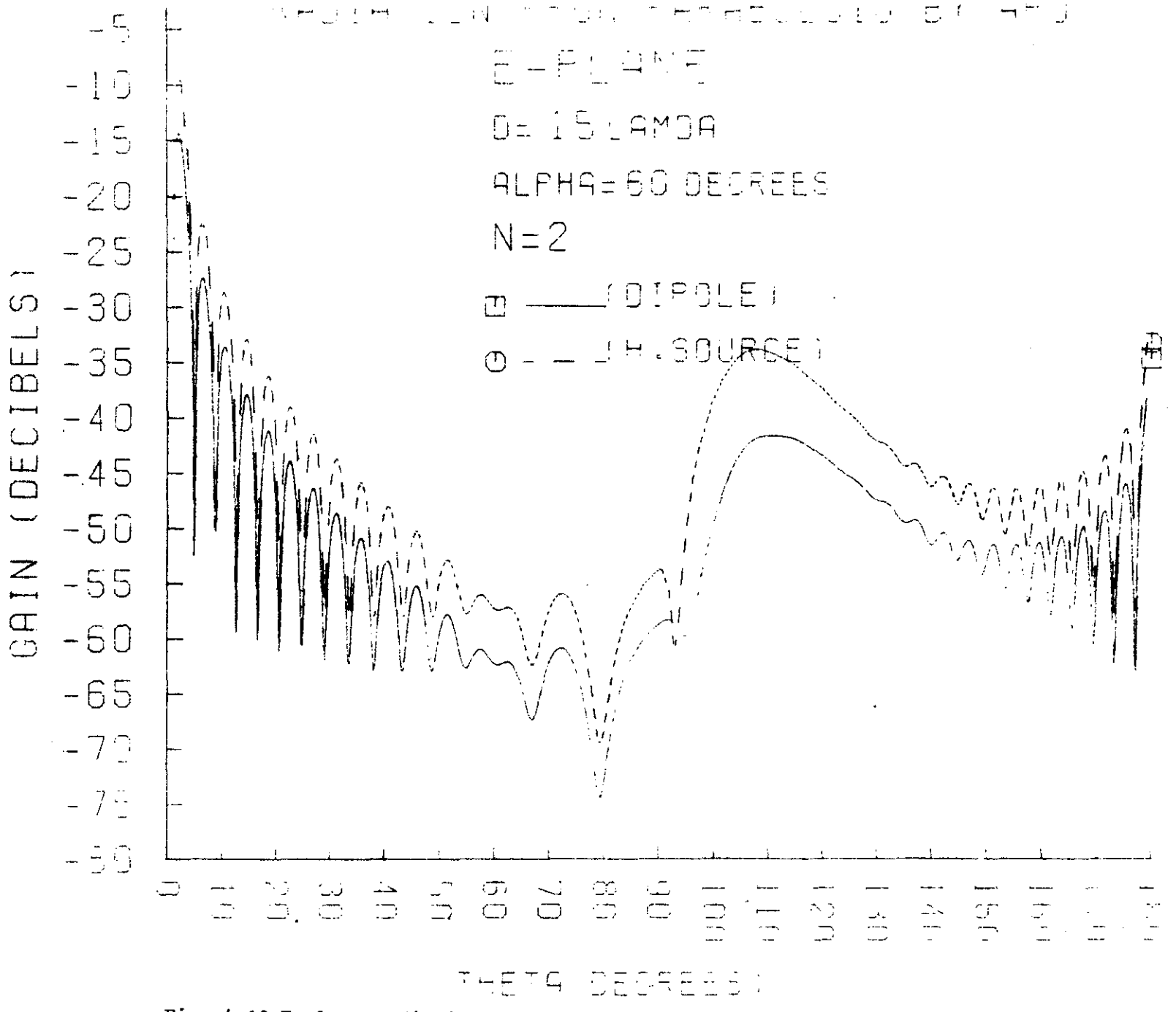

Fig. 4.13 E-plane radiation pattern. of a focus-fed paraboloid for dipole and Huygens source feeds.

COMPARISON OF GTD WITH APO FOR PARABOLOID
E-PLANE (H.SOURCE)
D= 15 LAMDA
ALPHA= 60 DEGREES
N=6
APO
GTD
GAIN (DECIBELS)
THETA (DEGREES)

HUYGENS SOURCE						DIPOLE				
n	T_F (dB)	Gain (dB)	F/B (dB)	first sidelobe level (dB)		T_F (dB)	Gain (dB)	F/B (dB)	first sidelobe level (dB)	
				E-plane	H-plane				E-plane	H-plane
2	- 6	32.56	33.3	-22.51	-22.44	- 8.44	31.48	34.7	-27.45	-21.36
4	-12	32.46	37.0	-26.21	-26.15	-14.44	31.51	38.55	-31.29	-25.2
6	-18	31.91	41.0	-30.22	-30.15	-20.44	31.08	42.67	-35.41	-29.32

Table 4.3

Influence of n on antenna performance parameters

$D/\lambda = 15$, $\alpha = 60^{\circ}$.

REFERENCES

1. W.V.T. Rusch, "Numerical and Asymptotic Techniques in Electromagnetics", ed. by R. Mittra, Berlin; Springer Verlag, 1975 Ch. 7, pp. 217-256.

2. J.B. Keller, "Diffraction by an Aperture", Journal of Applied Physics, vol. 28, no. 4, April 1957, pp. 426-444.

3. J.B. Keller, R.M. Lewis, B.D. Seckler, "Diffraction by an Aperture II", Journal of Applied Physics, vol. 28, nr. 5, May 1957, pp. 570-579.

4. R.M. Lewis, J. Boersma, "Uniform Asymptotic Theory of Edge Diffraction", J. of Mathematical Physics, vol. 10, nr. 12, December 1969, pp. 2291-2305.

5. R.G. Kouyoumjian, "Numerical and Asymptotic Techniques in Electromagnetics", ed. by R. Mittra. Berlin; Springer Verlag, 1975, Ch. 6, pp. 165-215.

6. IEEE Proceedings, Special issue on rays and beams, November 1974.

7. P.A.J. Ratnasiri, R.G. Kouyoumjian, P.H. Pathak, "The Wide Angle Side Lobes of Reflector Antennas", Ohio State Univ., Electroscience Lab., Technical Rep. 2183-1, March 1970.

8. W.V.T. Rusch, "Antenna Notes", Electromagnetics Institute, Technical University of Denmark, Lyngby, NB84, 1974, Vol. II.

9. C.A. Mentzer, L. Peters jr., "A GTD Analysis of the Far-Out Sidelobes of Cassegrain Antennas", IEEE Trans. Antennas Prop., vol. AP-23, pp. 702-709, September 1975.

10. B. Claydon, G.L. James, "Asymptotic Methods for the Prediction of Dual-Reflector-Antenna Efficiency", Proc. IEE, vol. 122, no. 12, December 1975, pp. 1359-1362.

11. C.M. Knop, "An Extension of Rusch's Asymptotic Physical Optics Diffraction Theory of a Paraboloid Antenna", IEEE Trans. Antennas and Prop., Vol. AP-23, September 1975, pp. 741-743.

12. C.E. Ryan and L. Peters, "Evaluation of Edge Diffracted Fields Including Equivalent Currents for the Caustic Regions", IEEE Trans. on Antennas and Prop., vol. AP-17, nr. 3, May 1969, pp. 292-299 (see also the correction, vol. AP-18, nr. 2, March 1970, p. 275).

13. G.L. James and V. Kerdemelidis, "Reflector Antenna Radiation Pattern Analysis by Equivalent Edge Currents", IEEE Trans. Antennas and Prop., vol. AP-21, nr. 1, Jan. 1973, pp. 19-24 (see also the comments, vol. AP-21, nr. 5, Sept. 1973, p. 756).

14. E.F. Knott and T.B.A. Senior, "Equivalent Currents for a Ring Discontinuity", IEEE Trans. Antennas and Prop., vol. AP-21, no. 5, Sept. 1973, pp. 693-695.

15. S. Silver, Microwave Antenna Theory and Design, Mc Graw Hill, New York, 1948.

16. W.V.T. Rusch and P.D. Potter, "Analysis of Reflector Antennas" Academic Press, New York, 1970.

17. R.E. Collin and F.J. Zucker, "Antenna Theory", New York, Mc Graw Hill 1969, ch. 17, pt. 2.

18. L.B. Felsen and N. Marcuvitz, "Radiation and Scattering of Waves", Prentice Hall, 1973, ch. 4.

19. N. Bleistein, "Uniform Asymptotic Expansions of Integrals with Stationary Point near Algebraic Singularity", Comm. on Pure and Applied Math., vol. XIX, no. 4, pp. 353-370, 1966.

20. N. Bleistein and R.A. Handelsman, "Uniform Asymptotic Expansions of Double Integrals", Journal of Math. Analysis and Applications, Vol. 27, 1969, pp. 434-453.

21. E.T. Copson, "Asymptotic Expansions", Cambridge, Cambridge University Press, 1965.

22. H. Jeffreys, "Asymptotic Approximations", Oxford, Clarendon Press, 1962.

23. M. Abramowitz and I.A. Stegun, "Handbook of Mathematical Functions", New York, Dover, 1965, ch. 9.

24. C.M. Knop, "On the Front to Back Ratio of a Parabolic Dish Antenna", IEEE Trans. Antennas and Prop., vol. AP-24, no. 1, January 1976, pp. 109-111.

25. M. Safak, "Calculation of Radiation Patterns of Paraboloidal Reflectors by High Frequency Asymptotic Techniques", Electronics Letters, 1976, vol. 12, pp. 229-231.

26. M. Safak and P. Delogne, "Cross-polarization in Cassegrainian and Front-Fed Paraboloidal Antennas", to be published in IEEE Trans. Antennas and Prop. in 1976.

APPENDIX A

Diffraction from a curved edge

Diffracted field at a point Q at the edge of a perfectly conducting half plane may be written as [5]

$$\begin{bmatrix} E_{\parallel}^{d} \\ E_{\perp}^{d} \end{bmatrix} = \begin{bmatrix} D_s & 0 \\ 0 & D_h \end{bmatrix} \begin{bmatrix} E_{\parallel}^{i} \\ E_{\perp}^{i} \end{bmatrix} \sqrt{\frac{\rho c}{s(\rho_c + s)}}\; e^{-jks} \qquad \text{(A-1)}$$

where s is the distance from the observation point P to the diffracting point Q at the edge (See Fig. A-1).

If $\hat{e}$ is the unit tangent vector to the edge at Q and $\hat{s}^i$ and $\hat{s}$ are respectively the unit vectors in the direction of incident and diffracted field, then

$$E_{\parallel}^{i} = \bar{E}^{i}.\hat{e} \qquad \text{(A-2a)}$$

$$E_{\perp}^{i} = \bar{E}^{i}.(\hat{e} \times \hat{s}^{i}) \qquad \text{(A-2b)}$$

$$E_{\parallel}^{d} = \bar{E}^{d}.\hat{e} \qquad \text{(A-2c)}$$

$$E_{\perp}^{d} = \bar{E}^{d}.(\hat{e} \times \hat{s}) \qquad \text{(A-2d)}$$

ρ_c is the caustic distance defined by

$$\frac{1}{\rho_c} = \frac{1}{\rho_e^{i}} - \frac{\hat{n}_e.(\hat{s}^{i} - \hat{s})}{K \sin^2\beta_o} \qquad \text{(A-3)}$$

where

ρ_e^{i} : radius of curvature of the incident field at the diffracting point at the edge in the plane containing the incident ray and the tangent to the edge (in the plane formed by $\hat{e}$ and $\hat{s}^i$). (For the incident spherical wave, it is equal to the distance from the phase center of the source to the edge).

$\hat{n}_e$: Unit normal vector to the edge at the point of diffraction directed outwards from the center of curvature.

$\hat{s}^i, \hat{s}$: unit vectors along the incident and diffracted rays respectively.

K : radius of curvature of the edge at the point of diffraction.

β_o : angle between the edge tangent and the incident ray at the point of diffraction. (all incident and diffracted rays in this work have $\beta_o = \pi/2$).

Diffraction coefficients considered in this work may be expressed as

$$D_{s}^{h} = \frac{-e^{-j\frac{\pi}{4}}}{2\sqrt{2\pi k}\sin\beta_o}\left[\frac{F(z^{i}e^{j\frac{\pi}{4}})}{\cos\frac{\gamma_d-\gamma_i}{2}} \pm \frac{F(z^{r}e^{j\frac{\pi}{4}})}{\cos\frac{\gamma_d+\gamma_i}{2}}\right] \tag{A-4}$$

where

$$z_{r}^{i} = \sqrt{2kL_{r}^{i}}\left|\cos\frac{\gamma_d \mp \gamma_i}{2}\right| \tag{A-4a}$$

and γ_i and γ_d denote the angles of incidence and diffraction respectively, in the plane perpendicular to the edge at the point of diffraction, measured from a reference direction.

For paraboloidal reflectors, the incident source field has always spherical wavefront. For this reason, parameters L^i and L^r are simply given by

$$L^{i} = \rho_c\Big|_{SB} = \rho_e^{i} = \text{value of the caustic distance } \rho_c \text{ at the shadow boundary} \tag{A-5}$$

$$L^{r} = \rho_c\Big|_{RB} = \text{value of } \rho_c \text{ at the reflection boundary.} \tag{A-6}$$

As for the so-called transition function, it is defined by

$$F(z\,e^{\pm j\frac{\pi}{4}}) = 2z\,e^{\pm j(z^2+\frac{\pi}{2})}\int_{z}^{\infty} e^{\mp jt^2}dt$$

$$= 2\sqrt{\pi}\,z\,e^{\pm j(z^2+\frac{\pi}{4})}\,Q(z\,e^{\pm j\frac{\pi}{4}}) \tag{A-7}$$

where

$$Q(z\,e^{\pm j\frac{\pi}{4}}) = \frac{e^{\pm j\frac{\pi}{4}}}{\sqrt{\pi}}\int_{z}^{\infty} e^{\mp jt^2}dt$$

$$= U(-z) + (\operatorname{sgn} z)\frac{e^{\pm j\frac{\pi}{4}}}{\sqrt{\pi}}\int_{|z|}^{\infty} e^{\mp jt^2}dt \tag{A-8}$$

It can easily been shown that [18]

$$Q(0) = \frac{1}{2} \tag{A-9}$$

and

$$Q\left(z\, e^{\pm j\frac{\pi}{4}}\right) \sim U(-z) + \frac{e^{\mp j\left(z^2+\frac{\pi}{4}\right)}}{2\sqrt{\pi}\, z} \qquad |z| \longrightarrow \infty \tag{A-10}$$

From Eqs. A-7 and A-10, it is evident that for positive large z, the transition function approaches to unity.

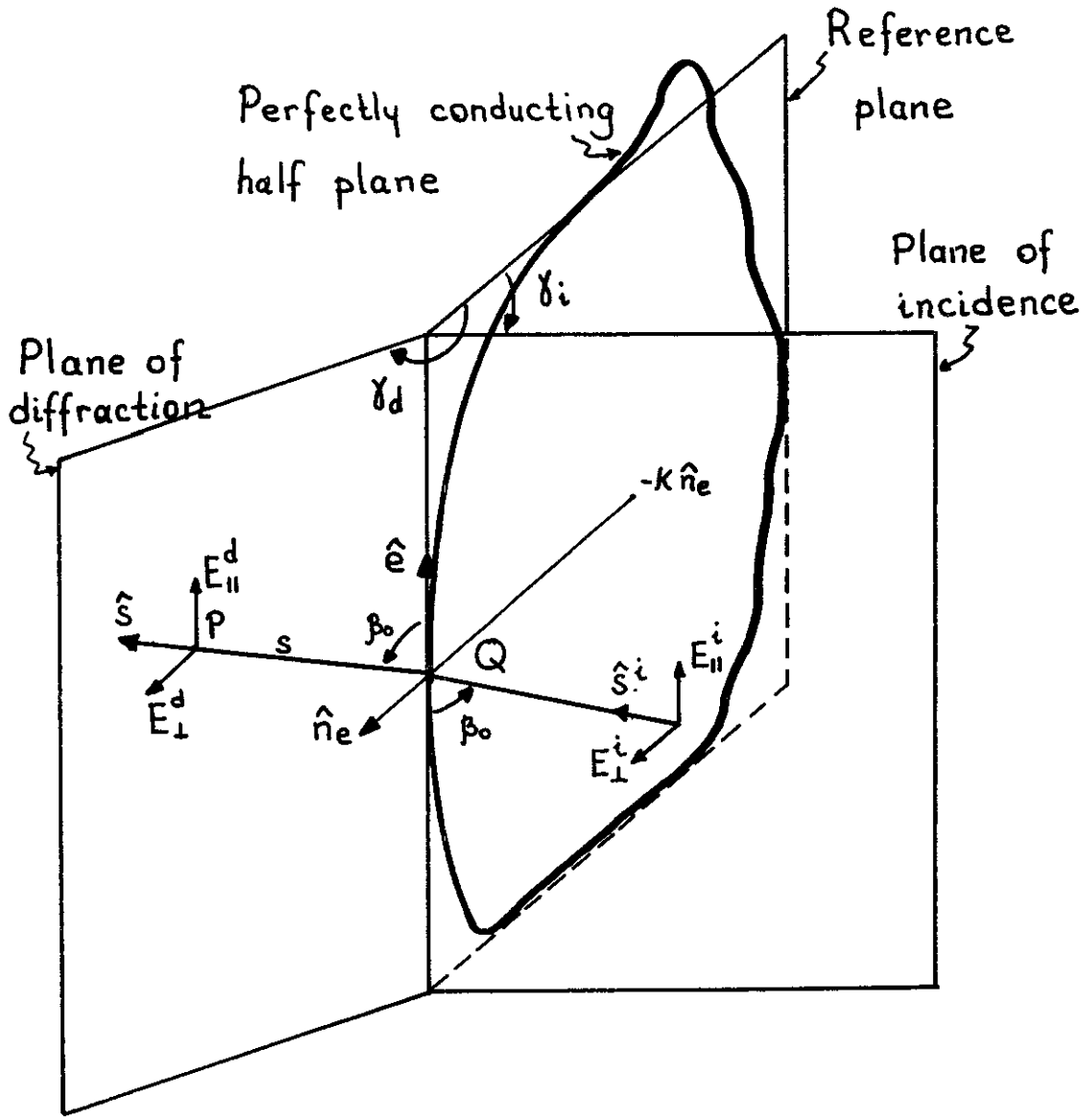

Fig. A.1 Diffraction at Q.

APPENDIX B

Coordinate transformations

$(x,y,z) \rightleftharpoons (\rho,\theta,\phi)$

$$\hat{x} = \hat{\rho}\sin\theta\cos\phi + \hat{\theta}\cos\theta\cos\phi - \hat{\phi}\sin\phi$$
$$\hat{y} = \hat{\rho}\sin\theta\sin\phi + \hat{\theta}\cos\theta\sin\phi + \hat{\phi}\cos\phi$$
$$\hat{z} = \hat{\rho}\cos\theta - \hat{\theta}\sin\theta$$

$$\hat{\rho} = \hat{x}\sin\theta\cos\phi + \hat{y}\sin\theta\sin\phi + \hat{z}\cos\theta$$
$$\hat{\theta} = \hat{x}\cos\theta\cos\phi + \hat{y}\cos\theta\sin\phi - \hat{z}\sin\theta$$
$$\hat{\phi} = -\hat{x}\sin\phi + \hat{y}\cos\phi$$

$(x,y,z) \rightleftharpoons (R,\Theta,\Phi)$

$$\hat{x} = \hat{R}\sin\Theta\cos\Phi + \hat{\Theta}\cos\Theta\cos\Phi - \hat{\Phi}\sin\Phi$$
$$\hat{y} = \hat{R}\sin\Theta\sin\Phi + \hat{\Theta}\cos\Theta\sin\Phi + \hat{\Phi}\cos\Phi$$
$$\hat{z} = \hat{R}\cos\Theta - \hat{\Theta}\sin\Theta$$

$$\hat{R} = \hat{x}\sin\Theta\cos\Phi + \hat{y}\sin\Theta\sin\Phi + \hat{z}\cos\Theta$$
$$\hat{\Theta} = \hat{z}\cos\Theta\cos\Phi + \hat{y}\cos\Theta\sin\Phi - \hat{z}\sin\Theta$$
$$\hat{\Phi} = -\hat{x}\sin\Phi + \hat{y}\cos\Phi$$

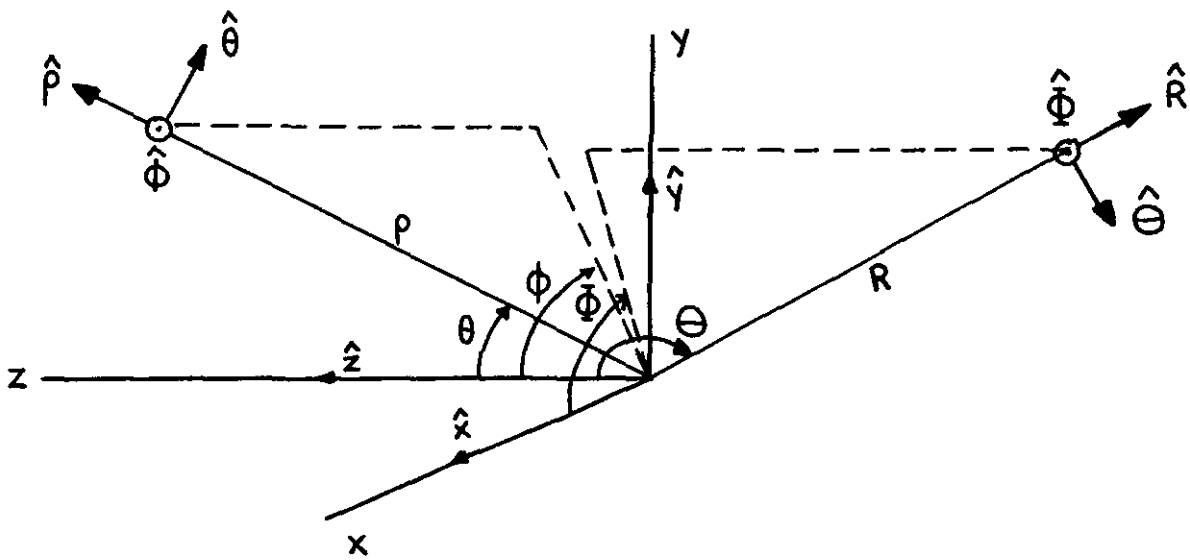

Fig. B.1 Unit vectors in different coordinate systems.

APPENDIX C

Stationary phase evaluation of finite integrals

We shall consider the integrals of the type

$$I(\Omega) = \int_a^b f(x)\, e^{j\psi(x)}\, dx = \int_a^b f(x)\, e^{j\Omega q(x)}\, dx \qquad \text{(C-1)}$$

where Ω is a positive large quantity and a and b are finite. f(x) and q(x) are slowly varying functions of the real variable x and q(x) is a real function. It may be shown that for $\Omega \to \infty$ the above integral can be approximated by ([18], [21])

$$I(\Omega) \sim I_s(\Omega)\, U[(x_s-a)(b-x_s)] + I_e(\Omega) + O(\Omega^{-\frac{3}{2}}) \qquad \text{(C-2)}$$

where U(α) is the Heaviside function defined by

$$U(\alpha) = \begin{cases} 1 & \alpha > 0 \\ 0 & \alpha < 0 \end{cases} \qquad \text{(C-3)}$$

$I_s(\Omega)$ is the lowest-order contribution from the stationary point x_s (for which $\psi_x(x_s) = 0$, $a < x_s < b$)

$$I_s(\Omega) = \sqrt{\frac{2\pi}{|\psi_{xx}(x_s)|}}\, f(x_s)\, e^{j\left[\psi(x_s) \pm \frac{\pi}{4}\right]} \qquad \psi_{xx}(x_s) \gtrless 0 \qquad \text{(C-4)}$$

and $I_e(\Omega)$ is the lowest-order contribution from the end-points

$$I_e(\Omega) = \frac{f(b)}{j\psi_x(b)}\, e^{j\psi(b)} - \frac{f(a)}{j\psi_x(a)}\, e^{j\psi(a)} \qquad \text{(C-5)}$$

If the integration interval contains several stationary points, $I_s(\Omega)$ is the sum of the corresponding terms of each x_s. When x_s coincides with either of the end-points a or b, the corresponding end-point contribution in Eq. C-5 is omitted and the stationary point contribution in Eq. C-4 is halved. If the interval contains no stationary point, U vanishes and the integral is approximated by the end-point contributions. In the case that an end-point moves to infinity, the corresponding contribution is omitted.

The above approach fails when x_s approaches one of the end-points; when x_s moves continuously toward and accross one of the endpoints, the term $I_s(\Omega)$ is

discontinuous since the saddle point disappears from the integration interval and $I_e(\Omega)$ diverges since $\psi_x(x_s) \to \psi_x\{{a \atop b}\} \to 0$ as $x_s \to \{{a \atop b}\}$. For this case a more careful approach is necessary. To simplify the discussion, let us consider the case where x_s moves towards and across a.

The integral in Eq. C-1 can then be approximated by [18]

$$I(\Omega) \sim e^{j[\psi(x_s) \pm \frac{\pi}{4}]} \left\{ f(x_s) h_s Q(s_a e^{\mp j\frac{\pi}{4}}) + \frac{e^{\pm j(s_a^2 + \frac{\pi}{4})}}{2\sqrt{\pi}\, s_a} \left[f(a) h_a - f(x_s) h_s \right] \right\}$$

$$+ \frac{f(b)}{j\psi_x(b)} e^{j\psi(b)} = I_e(\Omega) + I_s(\Omega)\, W(s_a e^{\mp j\frac{\pi}{4}})$$

$$\psi_{xx}(x_s) \gtrless 0 \qquad \text{(C-6)}$$

where

$$s_a = \pm \sqrt{|\psi(x_s) - \psi(a)|} \qquad (a - x_s) \gtrless 0 \qquad \text{(C-7)}$$

$$h_s = \sqrt{\frac{2\pi}{|\psi_{xx}(x_s)|}} = h_a \Big|_{x_s = a} \qquad \text{(C-8)}$$

$$h_a = \frac{\pm 2\sqrt{\pi}\, s_a}{\psi_x(a)} \qquad \psi_{xx}(x_s) \gtrless 0 \qquad \text{(C-9)}$$

$$W(s_a e^{\mp j\frac{\pi}{4}}) = Q(s_a e^{\mp j\frac{\pi}{4}}) - \frac{e^{\pm j(s_a^2 + \frac{\pi}{4})}}{2\sqrt{\pi}\, s_a}$$

$$= \frac{e^{\mp j\frac{\pi}{4}}}{\sqrt{\pi}} \left[\int_{s_a}^{\infty} e^{\pm j t^2} dt - \frac{e^{\pm j(s_a^2 + \frac{\pi}{2})}}{2 s_a} \right] \qquad \text{(C-10)}$$

Q function is defined by Eq. A-8. For $|s_a|$ large, from Eq. A-10,

$$W(s_a e^{\mp j\frac{\pi}{4}}) \sim U(-s_a) \qquad |s_a| \longrightarrow \infty \qquad \text{(C-11)}$$

When $x_s \to a$ ($s_a \to 0$), $Q(0) = \frac{1}{2}$ (Eq. A-9) and Eq. C-6 reduces to the coincident endpoint and stationary point contributions

$$I(\Omega) \sim \frac{1}{2}\sqrt{\frac{2\pi}{|\psi_{xx}(x_s)|}}\, f(x_s)\, e^{j[\psi(x_s) \pm \frac{\pi}{4}]} + \frac{f(b)}{j\psi_x(b)}\, e^{j\psi(b)} \qquad \psi_{xx}(x_s) \gtrless 0 \quad \text{(C-12)}$$

It is thus interesting to note that, in the case of the existance of a stationary point moving towards and across an endpoint, the stationary point contribution is multiplied by a function, W, removing the singularity at the considered endpoint (Eq. C-6).

In the case where x_s approaches b, s_a should be replaced by s_b, defined as

$$s_b = \pm\sqrt{|\psi(x_s) - \psi(b)|} \qquad (x_s - b) \gtrless 0 \quad \text{(C-13)}$$

APPENDIX D

From the integral definition of Bessel functions [23]

$$J_m(\beta) = \frac{1}{2\pi j^m} \int_0^{2\pi} \cos mt \; e^{j\beta \cos t} \, dt \tag{D-1}$$

one can easily find that

$$2\pi j^m J_m(\beta) \begin{Bmatrix} \cos m\bar{\Phi} \\ \sin m\bar{\Phi} \end{Bmatrix} = \int_0^{2\pi} \begin{Bmatrix} \cos m\phi \\ \sin m\phi \end{Bmatrix} e^{j\beta \cos(\bar{\Phi}-\phi)} \, d\phi \tag{D-2}$$

Similarly, using the trigonometric identity

$$\begin{Bmatrix} \cos^2\phi \\ \sin^2\phi \end{Bmatrix} = \frac{1}{2}\left(1 \pm \cos 2\phi\right) \tag{D-3}$$

and utilising Eqs. D-1 and D-2,

$$\int_0^{2\pi} \begin{Bmatrix} \cos^2\phi \\ \sin^2\phi \end{Bmatrix} e^{j\beta \cos(\bar{\Phi}-\phi)} \, d\phi = \pi\left[J_0(\beta) \mp \cos 2\bar{\Phi} J_2(\beta)\right] \tag{D-4}$$

On the other hand, owing to the trigonometric identities

$$\sin(A \pm B) = \sin A \cos B \pm \cos A \sin B \tag{D-5}$$

$$\cos(A \pm B) = \cos A \cos B \mp \sin A \sin B \tag{D-6}$$

and the Eqs. D-1 and D-2, it is readily found that

$$\int_0^{2\pi} \begin{Bmatrix} \cos\phi \\ \sin\phi \end{Bmatrix} \cos(\bar{\Phi}-\phi) \, e^{j\beta \cos(\bar{\Phi}-\phi)} \, d\phi = \pi\left[J_0(\beta) - J_2(\beta)\right] \begin{Bmatrix} \cos\bar{\Phi} \\ \sin\bar{\Phi} \end{Bmatrix} \tag{D-7}$$

$$\int_0^{2\pi} \begin{Bmatrix} \cos\phi \\ \sin\phi \end{Bmatrix} \sin(\bar{\Phi}-\phi) \, e^{j\beta \cos(\bar{\Phi}-\phi)} \, d\phi = \pi\left[J_0(\beta) + J_2(\beta)\right] \begin{Bmatrix} \sin\bar{\Phi} \\ -\cos\bar{\Phi} \end{Bmatrix} \tag{D-8}$$

$$\int_0^{2\pi} \begin{Bmatrix} \cos\phi \\ \sin\phi \end{Bmatrix} \cos(\bar{\Phi}+\phi) \, e^{j\beta \cos(\bar{\Phi}-\phi)} \, d\phi = \pi\left[J_0(\beta) + J_2(\beta)(1 \mp 2\cos 2\bar{\Phi})\right] \begin{Bmatrix} \cos\bar{\Phi} \\ -\sin\bar{\Phi} \end{Bmatrix} \tag{D-9}$$

$$\int_0^{2\pi} \begin{Bmatrix} \cos\phi \\ \sin\phi \end{Bmatrix} \sin(\bar{\Phi}+\phi) \, e^{j\beta \cos(\bar{\Phi}-\phi)} \, d\phi = \pi\left[J_0(\beta) - J_2(\beta)(1 \pm 2\cos 2\bar{\Phi})\right] \begin{Bmatrix} \sin\bar{\Phi} \\ \cos\bar{\Phi} \end{Bmatrix} \tag{D-10}$$

APPENDIX E

Derivatives of the phase function

From Eq. 4.12

$$\Psi(\theta,\phi) = k\rho\left[1 - \cos\theta\cos\Theta - \sin\theta\sin\Theta\cos(\Phi-\phi)\right] \tag{E-1}$$

$$\Psi_{\phi}(\theta,\phi) = -k\rho\sin\theta\sin\Theta\sin(\Phi-\phi) \tag{E-2}$$

$$\Psi_{\phi\phi}(\theta,\phi) = k\rho\sin\theta\sin\Theta\cos(\Phi-\phi) \tag{E-3}$$

$$\Psi_{\phi\theta}(\theta,\phi) = \Psi_{\theta\phi}(\theta,\phi) = -k\rho\sin\Theta\sin(\Phi-\phi) \tag{E-4}$$

$$\Psi_{\theta}(\theta,\phi) = k\rho(1+\cos\Theta)\left[\tan\frac{\theta}{2} - \tan\frac{\Theta}{2}\cos(\Phi-\phi)\right] \tag{E-5}$$

$$\Psi_{\theta\theta}(\theta,\phi) = k\rho(1+\cos\Theta)\left[\frac{1}{2}\sec^2\frac{\theta}{2} + \tan^2\frac{\theta}{2} - \tan\frac{\theta}{2}\tan\frac{\Theta}{2}\cos(\Phi-\phi)\right] \tag{E-6}$$

At $\phi = \phi_{\pm}$ making Eq. E-2 stationary, i.e.

$$\phi_{+} = \Phi \tag{E-7}$$

$$\phi_{-} = \Phi + \pi \tag{E-8}$$

the above equations reduce to

$$\Psi(\theta,\phi_{\pm}) = 2k\rho\sin^2\frac{\theta \mp \Theta}{2} \tag{E-9}$$

$$\Psi_{\phi\phi}(\theta,\phi_{\pm}) = \pm k\rho\sin\theta\sin\Theta \tag{E-10}$$

$$\Psi_{\theta}(\theta,\phi_{\pm}) = 2k\rho\cos\frac{\Theta}{2}\sec\frac{\theta}{2}\sin\frac{\theta \mp \Theta}{2} \tag{E-11}$$

$$\Psi_{\theta\theta}(\theta,\phi_{\pm}) = 2k\rho\left(\cos\frac{\Theta}{2}\sec\frac{\theta}{2}\right)^2\left[1 - \frac{\cos(\theta \mp \frac{\Theta}{2})}{2\cos\frac{\Theta}{2}}\right]$$

$$= 2k\rho\cos^2\frac{\Theta}{2}\left[\frac{1}{2}\sec^2\frac{\theta}{2} + \tan^2\frac{\theta}{2} \mp \tan\frac{\theta}{2}\tan\frac{\Theta}{2}\right] \tag{E-12}$$

$$\Psi_{\theta\phi}(\theta,\phi_{\pm}) = \Psi_{\phi\theta}(\theta,\phi_{\pm}) = \Psi_{\phi}(\theta,\phi_{\pm}) = 0 \tag{E-13}$$

At $\theta = \pm\Theta$ rendering $\psi_\theta(\theta,\phi\pm)$ stationary, Eqs. E-9 to 13 may be written as

$$\psi_{\phi\phi}(\pm\Theta,\phi_\pm) = k\rho(\Theta)\sin^2\Theta \tag{E-14}$$

$$\psi_{\theta\theta}(\pm\Theta,\phi_\pm) = k\rho(\Theta) \tag{E-15}$$

$$\psi(\pm\Theta,\phi_\pm)=\psi_\phi(\pm\Theta,\phi_\pm)=\psi_\theta(\pm\Theta,\phi_\pm)=\psi_{\theta\phi}(\pm\Theta,\phi_\pm)=\psi_{\phi\theta}(\pm\Theta,\phi_\pm)=0 \tag{E-16}$$

where

$$\rho(\Theta) = \rho\big|_{\theta=\Theta} = \frac{2f}{1+\cos\Theta} \tag{E-17}$$

Finally, at the end points $(\rho_o,\alpha,\phi\pm)$, Eqs. E-9 to 13 become

$$\psi(\alpha,\phi_\pm) = 2k\rho_o \sin^2\frac{\alpha\mp\Theta}{2} \tag{E-18}$$

$$\psi_{\phi\phi}(\alpha,\phi_\pm) = \pm k\rho_o \sin\alpha\sin\Theta \tag{E-19}$$

$$\psi_\theta(\alpha,\phi_\pm) = 2k\rho_o K_e^{\pm} \sin\frac{\alpha\mp\Theta}{2} \tag{E-20}$$

$$\psi_{\theta\theta}(\alpha,\phi_\pm) = 2k\rho_o K_e^{\pm 2}\left[1-\cos(\alpha\mp\Theta/2)/2\cos\frac{\Theta}{2}\right] \tag{E-21}$$

$$\psi_\phi(\alpha,\phi\pm) = \psi_{\phi\theta}(\alpha,\phi_\pm) = \psi_{\theta\phi}(\alpha,\phi_\pm) = 0 \tag{E-22}$$

where $K_e^{\pm}$ is defined by

$$K_e^{\pm} = \sec\frac{\alpha}{2}\cos\frac{\Theta}{2} \tag{E-23}$$

APPENDIX F

Integral kernels

From Eq. 4.11

$$\left.\begin{matrix} f_\Theta(\theta,\phi) \\ f_\Phi(\theta,\phi) \end{matrix}\right\} = -\frac{jk\rho\sin\theta}{2\pi}\sqrt{G_f(\theta)}\left\{\begin{matrix} \cos\Theta\left[\sin\bar{\Phi} + (u_\theta - 1)\sin\phi\cos(\bar{\Phi}-\phi)\right] + \sin\Theta\tan\frac{\theta}{2}\,u_\theta\sin\phi \\ \cos\bar{\Phi} - (u_\theta - 1)\sin\phi\sin(\bar{\Phi}-\phi) \end{matrix}\right\} \qquad \text{(F-1)}$$

At $\phi = \phi \pm$, defined by Eqs. E-7 and E-8, the above equation reduces to

$$\left.\begin{matrix} f_\Theta(\theta,\phi_\pm) \\ f_\Phi(\theta,\phi_\pm) \end{matrix}\right\} = -\frac{jk\rho\sin\theta}{2\pi}\sqrt{G_f(\theta)}\left\{\begin{matrix} u_\theta\sin\bar{\Phi} \\ \cos\bar{\Phi} \end{matrix}\right\}\left\{\begin{matrix} \cos(\Theta \mp \frac{\theta}{2})/\cos\frac{\theta}{2} \\ 1 \end{matrix}\right\} \qquad \text{(F-2)}$$

At $(\rho, \pm\Theta, \phi\pm)$, Eq. F-2 may simply be written as

$$\left.\begin{matrix} f_\Theta(\pm\Theta,\phi_\pm) \\ f_\Phi(\pm\Theta,\phi_\pm) \end{matrix}\right\} = \mp\frac{jk\rho(\theta)\sin\Theta}{2\pi}\sqrt{G_f(\Theta)}\left\{\begin{matrix} u_\Theta\sin\bar{\Phi} \\ \cos\bar{\Phi} \end{matrix}\right\} \qquad \text{(F-3)}$$

where $\rho(\Theta)$ is defined by Eq. E-17.

Finally at the edge points $(\rho_o,\alpha,\phi\pm)$, Eq. F-2 becomes

$$\left.\begin{matrix} f_\Theta(\alpha,\phi_\pm) \\ f_\Phi(\alpha,\phi_\pm) \end{matrix}\right\} = -\frac{jk\rho_o\sin\alpha}{2\pi}\sqrt{G_f(\alpha)}\left\{\begin{matrix} u_\alpha\sin\bar{\Phi} \\ \cos\bar{\Phi} \end{matrix}\right\}\left\{\begin{matrix} K^{\pm}_{k\Theta} \\ K^{\pm}_{k\Phi} \end{matrix}\right\} \qquad \text{(F-4)}$$

where

$$\left.\begin{matrix} K^{\pm}_{k\Theta} \\ K^{\pm}_{k\Phi} \end{matrix}\right\} = \left\{\begin{matrix} \cos(\Theta \mp \frac{\alpha}{2})/\cos\frac{\alpha}{2} \\ 1 \end{matrix}\right\} \qquad \text{(F-5)}$$

APPENDIX G

The expression from Eq. 4.30

$$M^{\pm}(\Theta) = \int_0^{\alpha} \exp\left[-j\left\{\Psi_\theta(\alpha,\phi_\pm)(\theta-\alpha) + \frac{1}{2}\Psi_{\theta\theta}(\alpha,\phi_\pm)(\theta-\alpha)^2\right\}\right] d\theta \qquad \text{(G-1)}$$

by a change of variables may be written as

$$M^{\pm}(\Theta) = \int_0^{\alpha} \exp\left[-j\left\{-\Psi_\theta(\alpha,\phi_\pm)\,t + \frac{1}{2}\Psi_{\theta\theta}(\alpha,\phi_\pm)\,t^2\right\}\right] dt \qquad \text{(G-2)}$$

where the major contribution to the integral comes from the neigborhood of $t = 0$. For this reason, the upper integral limit is extended to infinity without much error.

Bearing in mind that $\psi_{\theta\theta}(\alpha,\phi_\pm) > 0$ (Eq. E-21) and using the identity

$$\frac{1}{2}\Psi_{\theta\theta}(\alpha,\phi_\pm)\,t^2 - \Psi_\theta(\alpha,\phi_\pm)\,t = \left(\sqrt{\frac{|\Psi_{\theta\theta}(\alpha,\phi_\pm)|}{2}}\,t - d_\pm\right)^2 - d_\pm^2 \qquad \text{(G-3)}$$

where

$$d_\pm = \frac{\Psi_\theta(\alpha,\phi_\pm)}{\sqrt{2|\Psi_{\theta\theta}(\alpha,\phi_\pm)|}} = \sqrt{\frac{2kp_0\left|\cos\frac{\Theta}{2}\right|}{\left|2\cos\frac{\Theta}{2} - \cos\left(\alpha \mp \frac{\Theta}{2}\right)\right|}}\,\sin\frac{\alpha \mp \Theta}{2} \qquad \text{(G-4)}$$

Substitution of Eq. G-3 into Eq. G-2, and another change of variables yield

$$M^{\pm}(\Theta) = \sqrt{\frac{2}{|\Psi_{\theta\theta}(\alpha,\phi_\pm)|}}\; e^{-jd_\pm^2} \int_{-d_\pm}^{\infty} e^{-jt^2} dt = \sqrt{\frac{2\pi}{|\Psi_{\theta\theta}(\alpha,\phi_\pm)|}}\; e^{j\left(d_\pm^2 - \frac{\pi}{4}\right)} Q\left(-d_\pm e^{j\frac{\pi}{4}}\right)$$

where the Q function is defined by Eq. A-8.

Argument of the Q function becomes negative in the shadow region accounting for the stationary point contribution which is spearately studied in section 4.2.2.a. For this reason, endpoint contribution may simply be written as

$$M^{\pm}(\Theta) = j\sqrt{\frac{2\pi}{|\Psi_{\theta\theta}(\alpha,\phi_\pm)|}}\; e^{j\left(d_\pm^2 + \frac{\pi}{4}\right)} Q\left(|d_\pm| e^{j\frac{\pi}{4}}\right) = \frac{F\left(|d_\pm| e^{j\frac{\pi}{4}}\right)}{-j\Psi_\theta(\alpha,\phi_\pm)}$$

(G-5)

It can easily be shown that as $d^{\pm} \to 0$ (i.e. in the shadow and reflection boundaries), $M^{\pm}(\theta)$ reduces to

$$M^{\pm}(\theta) = \frac{1}{2}\sqrt{\frac{2\pi}{|\psi_{\theta\theta}(\alpha,\phi\pm)|}}\; e^{-j\frac{\pi}{4}} \qquad \text{(G-6)}$$

which is equal to coincident end- and stationary points contributions as expected.

EINDHOVEN UNIVERSITY OF TECHNOLOGY
EINDHOVEN (THE NETHERLANDS)
DEPARTMENT OF ELECTRICAL ENGINEERING

Reports:

1: Dijk, J., M. Jeuken and E.J. Maanders
AN ANTENNA FOR A SATELLITE COMMUNICATION GROUND STATION (PROVISIONAL ELECTRICAL DESIGN). TH-Report 68-E-01. March 1968. ISBN 90-6144-001-7

2: Veefkind, A., J.H. Blom and L.H.Th. Rietjens
THEORETICAL AND EXPERIMENTAL INVESTIGATION OF A NON-EQUILIBRIUM PLASMA IN A MHD CHANNEL. (Submitted to the Symposium on a Magnetohydrodynamic Electrical Power Generation, Warsaw, Poland, 24-30 July, 1968. TH-Report 68-E-2. March 1968. ISBN 90-6144-002-5

3: Boom, A.J.W. van den and J.H.A.M. Melis
A COMPARISON OF SOME PROCESS PARAMETER ESTIMATING SCHEMES. TH-Report 68-E-03. September 1968. ISBN 90-6144-003-3

4: Eykhoff, P., P.J.M. Ophey, J. Severs and J.O.M. Oome
AN ELECTROLYTIC TANK FOR INSTRUCTIONAL PURPOSES REPRESENTING THE COMPLEX-FREQUENCY PLANE. TH-Report 68-E-04. September 1968. ISBN 90-6144-004-1

5: Vermij, L. and J.E. Daalder
ENERGY BALANCE OF FUSING SILVER WIRES SURROUNDED BY AIR. TH-Report 68-E-05. November 1968. ISBN 90-6144-005-X

6: Houben, J.W.M.A. and P. Massee
MHD POWER CONVERSION EMPLOYING LIQUID METALS. TH-Report 69-E-06. February 1969. ISBN 90-6144-006-8

7: Heuvel, W.M.C. van den and W.F.J. Kersten
VOLTAGE MEASUREMENT IN CURRENT ZERO INVESTIGATIONS. TH-Report 69-E-07. September 1969. ISBN 90-6144-007-6

8: Vermij, L.
SELECTED BIBLIOGRAPHY OF FUSES. TH-Report 69-E-08. September 1969. ISBN 90-6144-008-4

9: Westenberg, J.Z.
SOME IDENTIFICATION SCHEMES FOR NON-LINEAR NOISY PROCESSES. TH-Report 69-E-09. December 1969. ISBN 90-6144-009-2

10: Koop, H.E.M., J. Dijk and E.J. Maanders
ON CONICAL HORN ANTENNAS. TH-Report 70-E-10. February 1970. ISBN 90-6144-010-6

11: Veefkind, A.
NON-EQUILIBRIUM PHENOMENA IN A DISC-SHAPED MAGNETOHYDRODYNAMIC GENERATOR. TH-Report 70-E-11. March 1970. ISBN 90-6144-011-4

12: Jansen, J.K.M., M.E.J. Jeuken and C.W. Lambrechtse
THE SCALAR FEED. TH-Report 70-E-12. December 1969. ISBN 90-6144-012-2

13: Teuling, D.J.A.
ELECTRONIC IMAGE MOTION COMPENSATION IN A PORTABLE TELEVISION CAMERA. TH-Report 70-E-13. November 1970. ISBN 90-6144-013-0

EINDHOVEN UNIVERSITY OF TECHNOLOGY
EINDHOVEN (THE NETHERLANDS)
DEPARTMENT OF ELECTRICAL ENGINEERING

Reports:

14: Lorencin, M.
AUTOMATIC METEOR REFLECTIONS RECORDING EQUIPMENT. TH-Report 70-E-14. November 1970. ISBN 90-6144-014-9

15: Smets, A.J.
THE INSTRUMENTAL VARIABLE METHOD AND RELATED IDENTIFICATION SCHEMES. TH-Report 70-E-15. November 1970. ISBN 90-6144-015-7

16: White, Jr., R.C.
A SURVEY OF RANDOM METHODS FOR PARAMETER OPTIMIZATION. TH-Report 70-E-16. February 1971. ISBN 90-6144-016-5

17: Talmon, J.L.
APPROXIMATED GAUSS-MARKOV ESTIMATORS AND RELATED SCHEMES. TH-Report 71-E-17. February 1971. ISBN 90-6144-017-3

18: Kalášek, V.
MEASUREMENT OF TIME CONSTANTS ON CASCADE D.C. ARC IN NITROGEN. TH-Report 71-E-18. February 1971. ISBN 90-6144-018-1

19: Hosselet, L.M.L.F.
OZONBILDUNG MITTELS ELEKTRISCHER ENTLADUNGEN. TH-Report 71-E-19. March 1971. ISBN 90-6144-019-X

20: Arts, M.G.J.
ON THE INSTANTANEOUS MEASUREMENT OF BLOODFLOW BY ULTRASONIC MEANS. TH-Report 71-E-20. May 1971. ISBN 90-6144-020-3

21: Roer, Th.G. van de
NON-ISO THERMAL ANALYSIS OF CARRIER WAVES IN A SEMICONDUCTOR. TH-Report 71-E-21. August 1971. ISBN 90-6144-021-1

22: Jeuken, P.J., C. Huber and C.E. Mulders
SENSING INERTIAL ROTATION WITH TUNING FORKS. TH-Report 71-E-22. September 1971. ISBN 90-6144-022-X

23: Dijk, J. and E.J. Maanders
APERTURE BLOCKING IN CASSEGRAIN ANTENNA SYSTEMS. A REVIEW. TH-Report 71-E-23. September 1971. ISBN 90-6144-023-8

24: Kregting, J. and R.C. White, Jr.
ADAPTIVE RANDOM SEARCH. TH-Report 71-E-24. October 1971. ISBN 90-6144-024-6

25: Damen, A.A.H. and H.A.L. Piceni
THE MULTIPLE DIPOLE MODEL OF THE VENTRICULAR DEPOLARISATION. TH-Report 71-E-25. October 1971. ISBN 90-6144-025-4

26: Bremmer, H.
A MATHEMATICAL THEORY CONNECTING SCATTERING AND DIFFRACTION PHENOMENA, INCLUDING BRAGG-TYPE INTERFERENCES. TH-Report 71-E-26. December 1971. ISBN 90-6144-026-2

EINDHOVEN UNIVERSITY OF TECHNOLOGY
EINDHOVEN (THE NETHERLANDS)
DEPARTMENT OF ELECTRICAL ENGINEERING

Reports:

27: Bokhoven, W.M.G. van
METHODS AND ASPECTS OF ACTIVE RC-FILTERS SYNTHESIS. TH-Report 71-E-27. March 1972. ISBN 90-6144-027-0

28: Boeschoten, F.
TWO FLUIDS MODEL REEXAMINED FOR A COLLISIONLESS PLASMA IN THE STATIONARY STATE. TH-Report 72-E-28. February 1972. ISBN 90-6144-028-9

29: REPORT ON THE CLOSED CYCLE MHD SPECIALIST MEETING. Working Group of the Joint ENEA/IAEA International MHD Liaison Group. Eindhoven, The Netherlands, September 20,21 and 22, 1971. Edited by L.H.Th. Rietjens. TH-Report 72-E-29. April 1972. ISBN 90-6144-029-7

30: Kessel, C.G.M. van and J.W.M.A. Houben
LOSS MECHANISMS IN AN MHD GENERATOR. TH-Report 72-E-30. June 1972. ISBN 90-6144-030-0

31: Veefkind, A.
CONDUCTING GRIDS TO STABILIZE MHD GENERATOR PLASMAS AGAINST IONIZATION INSTABILITIES. TH-Report 72-E-31. September 1972. ISBN 90-6144-031-9

32: Daalder, J.E. and C.W.M. Vos
DISTRIBUTION FUNCTIONS OF THE SPOT DIAMETER FOR SINGLE- AND MULTI-CATHODE DISCHARGES IN VACUUM. TH-Report 73-E-32. January 1973. ISBN 90-6144-032-7

33: Daalder, J.E.
JOULE HEATING AND DIAMETER OF THE CATHODE SPOT IN A VACUUM ARC. TH-Report 73-E-33. January 1973. ISBN 90-6144-033-5

34: Huber, C.
BEHAVIOUR OF THE SPINNING GYRO ROTOR. TH-Report 73-E-34. February 1973. ISBN 90-6144-034-3

35: Bastian, C., F. Boeschoten, H. Hekman, H.P. Riske and A. van Iersel
THE VACUUM ARC AS A FACILITY FOR RELEVANT EXPERIMENTS IN FUSION RESEARCH. Annual Report 1972. Euratom-T.H.E. Group "Rotating Plasma". TH-Report 73-E-35. February 1973. ISBN 90-6144-035-1

36: Blom, J.A.
ANALYSIS OF PHYSIOLOGICAL SYSTEMS BY PARAMETER ESTIMATION TECHNIQUES. TH-Report 73-E-36. May 1973. ISBN 90-6144-036-X

37: This number was cancelled.

38: Andriessen, F.J., W. Boerman and I.F.E.M. Holtz
CALCULATION OF RADIATION LOSSES IN CYLINDRICAL SYMMETRICAL HIGH PRESSURE DISCHARGES BY MEANS OF A DIGITAL COMPUTER. TH-Report 73-E-38. August 1973. ISBN 90-6144-038-6

39: Dijk, J., C.T.W. van Diepenbeek, E.J. Maanders and L.F.G. Thurlings
THE POLARIZATION LOSSES OF OFFSET ANTENNAS. TH-Report 73-E-39. June 1973. ISBN 90-6144-039-4

EINDHOVEN UNIVERSITY OF TECHNOLOGY
EINDHOVEN (THE NETHERLANDS)
DEPARTMENT OF ELECTRICAL ENGINEERING

Reports:

40: Goes, W.P.
SEPARATION OF SIGNALS DUE TO ARTERIAL AND VENOUS BLOOD FLOW IN THE DOPPLER SYSTEM THAT USES CONTINUOUS ULTRASOUND. TH-Report 73-E-40. June 1973. ISBN 90-6144-040-8

41: Damen, A.A.H.
COMPARATIVE ANALYSIS OF SEVERAL MODELS OF THE VENTRICULAR DEPOLARISATION; INTRODUCTION OF A STRING MODEL. TH-Report 73-E-41. October 1973. ISBN 90-6144-041-6

42: Dijk, G.H.M. van
THEORY OF GYRO WITH ROTATING GIMBAL AND FLEXURAL PIVOTS. TH-Report 73-E-42. September 1973. ISBN 90-6144-042-4

43: Breimer, A.J.
ON THE IDENTIFICATION OF CONTINUOUS LINEAR PROCESSES. TH-Report 74-E-43. January 1974. ISBN 90-6144-043-2

44: Lier, M.C. van and R.H.J.M. Otten
C.A.D. OF MASKS AND WIRING. Th-Report 74-E-44. February 1974. ISBN 90-6144-044-0

45: Bastian, C., F. Boeschoten, H. Hekman, R. Komen, H.P. Riske and A. van Iersel
EXPERIMENTS WITH A LARGE SIZED HOLLOW CATHODE DISCHARGE FED WITH ARGON. Annual Report 1973. EURATOM-T.H.E. Group "Rotating Plasma". TH-Report 74-E-45. April 1974. ISBN 90-6144-045-9

46: Roer, Th.G. van de
ANALYTICAL SMALL-SIGNAL THEORY OF BARITT DIODES. TH-Report 74-E-46. May 1974. ISBN 90-6144-046-7

47: Leliveld, W.H.
THE DESIGN OF A MOCK CIRCULATION SYSTEM. TH-Report 74-E-47. June 1974. ISBN 90-6144-047-5

48: Damen, A.A.H.
SOME NOTES ON THE INVERSE PROBLEM IN ELECTRO CARDIOGRAPHY. TH-Report 74-E-48. July 1974. ISBN 90-6144-048-3

49: Meeberg, L. van de
A VITERBI DECODER. TH-Report 74-E-49. October 1974. ISBN 90-6144-049-1

50: Poel, A.P.M. van der
A COMPUTER SEARCH FOR GOOD CONVOLUTIONAL CODES. TH-Report 74-E-50. October 1974. ISBN 90-6144-050-5

51: Sampic, G.
THE BIT ERROR PROBABILITY AS A FUNCTION PATH REGISTER LENGTH IN THE VITERBI DECODER. TH-Report 74-E-51. October 1974. ISBN 90-6144-051-3

52: Schalkwijk, J.P.M.
CODING FOR A COMPUTER NETWORK. TH-Report 74-E-52. October 1974. ISBN 90-6144-052-1

EINDHOVEN UNIVERSITY OF TECHNOLOGY
EINDHOVEN (THE NETHERLANDS)
DEPARTMENT OF ELECTRICAL ENGINEERING

Reports:

53: Stapper, M.
MEASUREMENT OF THE INTENSITY OF PROGRESSIVE ULTRASONIC WAVES BY MEANS OF RAMAN-NATH DIFFRACTION. TH-Report 74-E-53. November 1974. ISBN 90-6144-053-X

54: Schalkwijk, J.P.M. and A.J. Vinck
SYNDROME DECODING OF CONVOLUTIONAL CODES. TH-Report 74-E-54. November 1974. ISBN 90-6144-054-8

55: Yakimov, A.
FLUCTUTATIONS IN IMPATT-DIODE OSCILLATORS WITH LOW q-SECTORS. TH-Report 74-E-55. November 1974. ISBN 90-6144-055-6

56: Plaats, J. van der
ANALYSIS OF THREE CONDUCTOR COAXIAL SYSTEMS. TH-Report 75-E-56. March 1975. ISBN 90-6144-056-4

57: Kooy, C.
RE-OPTICAL ANALYSIS OF A TWO DIMENSIONAL APERTURE RADIATION PROBLEM. TH-Report 75-E-57. April 1975. ISBN 90-6144-057-2

58: Schalkwijk, J.P.M., A.J. Vinck and L.J.A.E. Rust
ANALYSIS AND SIMULATION OF A SYNDROME DECODER FOR A CONSTRAINT LENGTH k = 5, RATE R = ½ BINARY CONVOLUTIONAL CODE. TH-Report 75-E-58. April 1975. ISBN 90-6144-058-0

59) Boeschoten, F. et al.
EXPERIMENTS WITH A LARGE SIZED HOLLOW CATHODE DISCHARGE FED WITH ARGON, II. Annual Report 1974. EURATOM-T.H.E. Group "Rotating Plasma". TH-report 75-E-59. June 1975. ISBN 90-6144-059-9

60) Maanders, E.J.
SOME ASPECTS OF GROUND STATION ANTENNAS FOR SATELLITE COMUNICATION. TH-report 75-E-60. August 1975. ISBN 90-6144-060-2
(This report has served as a thesis for the degree of Doctor of Applied Science at the University of Gent, Belgium, 1975)

61) Mawira, A. and J. Dijk
DEPOLARIZATION BY RAIN: Some Related Thermal Emission Considerations. TH-report 75-E-61. September 1975. ISBN 90-6144-061-0

62) Safak, M.
CALCULATION OF THE RADIATION PATTERNS OF PARABOLOIDAL REFLECTORS BY HIGH FREQUENCY ASYMPTOTIC TECHNIQUES.
TH-report 76-E-62. March 1976. ISBN 90-6144-062-9

63) Schalkwijk, J.P.M. and A.J. Vinck
SOFT DECISION SYNDROME DECODING.
TH-report 76-E-63. March 1976. ISBN 90-6144-063-7